AGU ADVANCING EARTH AND SPACE SCIENCE

Key Points:
- Hadal trench systems act as important hot spots for accumulation and retention of organic material in the deep sea
- The sediment and organic carbon accumulation in trench systems is partly mediated by ongoing material focusing
- Infrequent mass-wasting events triggered by earthquakes play a significant role on mass accumulation and organic carbon deposition

Supporting Information:
Supporting Information may be found in the online version of this article.

Correspondence to:
K. Oguri,
ogurik@biology.sdu.dk

Sediment Accumulation and Carbon Burial in Four Hadal Trench Systems

Kazumasa Oguri[1,2] , Pere Masqué[3,4,5], Matthias Zabel[6] , Heather A. Stewart[7], Gillian MacKinnon[8] , Ashley A. Rowden[9,10], Peter Berg[11], Frank Wenzhöfer[1,12,13] , and Ronnie N. Glud[1,14,15]

[1]Hadal & Nordcee, Department of Biology, University of Southern Denmark, Odense M, Denmark, [2]Research Institute for Global Change, Japan Agency for Marine-Earth Science and Technology, Yokosuka, Japan, [3]School of Natural Sciences, Centre for Marine Ecosystems Research, Edith Cowan University, Joondalup, WA, Australia, [4]Institute of Environmental Science and Technology and Physics Department, Universitat Autònoma de Barcelona, Bellaterra, Spain, [5]International Atomic Energy Agency Environment Laboratories, Monaco, Monaco, [6]Center for Marine Environmental Sciences, University of Bremen, Bremen, Germany, [7]British Geological Survey, Lyell Centre, Research Avenue South, Edinburgh, UK, [8]Scottish Universities Environmental Research Centre, Scottish Enterprise Technology Park, East Kilbride, UK, [9]National Institute of Water & Atmosphere Research, Wellington, New Zealand, [10]Victoria University of Wellington, Wellington, New Zealand, [11]Department of Environmental Sciences, University of Virginia, Charlottesville, VA, USA, [12]HGF-MPG Group for Deep Sea Ecology and Technology, Alfred-Wegener-Institute Helmholtz-Center for Polar and Marine Research, Bremerhaven, Germany, [13]Max-Planck-Institute for Marine Microbiology, Bremen, Germany, [14]Tokyo University of Marine Science and Technology, Tokyo, Japan, [15]DIAS, University of Southern Denmark, Odense M, Denmark

Abstract Hadal trenches are considered to act as depocenters for organic material, although pathways for the material transport and deposition rates are poorly constrained. Here we assess focusing, deposition and accumulation of material and organic carbon in four hadal trench systems underlying different surface ocean productivities; the eutrophic Atacama and Kuril-Kamchatka trenches, the mesotrophic Kermadec trench and the oligotrophic Mariana Trench. The study is based on the distributions of naturally occurring $^{210}Pb_{ex}$, ^{137}Cs and total organic carbon from recovered sediment cores and by applying previously quantified benthic mineralization rates. Periods of steady deposition and discreet mass-wasting deposits were identified from the profiles and the latter were associated with historic recorded seismic events in the respective regions. During periods without mass wasting, the estimated focusing factors along trench axes were elevated, suggesting more or less continuous downslope focusing of material toward the interior of the trenches. The estimated organic carbon deposition rates during these periods exhibited extensive site-specific variability, but were generally similar to values encountered at much shallower settings such as continental slopes and margins. Organic carbon deposition rates during periods of steady deposition were not mirrored by surface ocean productivity, but appeared confounded by local bathymetry. The inclusion of deposition mediated by mass-wasting events enhanced the sediment and organic carbon accumulations for the past ~150 years by up to a factor of ~4. Thus, due to intensified downslope material focusing and infrequent mass-wasting events, hadal trenches are important sites for deposition and sequestration of organic carbon in the deep sea.

Plain Language Summary Hadal trenches (>6,000 m water depth) occupy ~1% of the world's ocean floor yet are largely underexplored, but recent studies have shown that these environments are depocenters for organic material and microbial activity is intensified when compared to shallower abyssal plains. However, transport and accumulation of sediment material to these hadal trenches is poorly understood. This study investigates sedimentation and accumulation dynamics of organic carbon in trenches using results of radionuclide analysis (in sediment from the Atacama, Kuril-Kamchatka, Kermadec, and Mariana trenches). The analysis shows that trench sediments consist of discreet layers representing both periods of continuous deposition and sudden mass-wasting events often triggered by historic earthquakes. Down slope focusing of material, intensified the deposition along the trench axes. However, the deposition rates exhibited extensive site-specific variations that were partly related to mass-wasting events which greatly enhanced not only mass accumulation but also organic carbon accumulation at the trench axes. Our results illustrate that mass-wasting events play an important role on supplying organic carbon to hadal communities and suggest that hadal trenches might be quantitatively important for sediment and organic carbon sequestration in the deep sea.

Stewart, Gillian MacKinnon, Peter Berg, Ronnie N. Glud

Project Administration: Ashley A. Rowden, Frank Wenzhöfer, Ronnie N. Glud

Supervision: Ronnie N. Glud

Validation: Kazumasa Oguri, Pere Masqué, Matthias Zabel, Heather A. Stewart, Gillian MacKinnon, Ashley A. Rowden, Frank Wenzhöfer, Ronnie N. Glud

Visualization: Matthias Zabel, Heather A. Stewart

Writing – original draft: Kazumasa Oguri, Frank Wenzhöfer, Ronnie N. Glud

Writing – review & editing: Kazumasa Oguri, Pere Masqué, Matthias Zabel, Heather A. Stewart, Gillian MacKinnon, Ashley A. Rowden, Peter Berg, Frank Wenzhöfer, Ronnie N. Glud

1. Introduction

The hadal zone is defined as regions with water depths exceeding 6,000 m and covers approximately 1% of the ocean floor (Harris et al., 2014). The most prominent hadal environments stretch along tectonic subduction zones, where they form long, narrow trench systems. Generally, the vertical transport of organic material from the surface ocean attenuates strongly with ocean depth (Berger et al., 1987), but during the past two decades it has been realized that hadal trenches can act as depocenters for organic material (Danovaro et al., 2003; Ichino et al., 2015; Xu et al., 2021). In addition, some trench sediments hold surprisingly high levels of microbial and meiofaunal biomass (e.g., Brandt et al., 2020; Itoh et al., 2011; Schauberger et al., 2021; Zabel et al., 2022) and hadal sediments appear to express elevated O_2 consumption rates as compared to adjacent abyssal sites with water depths of 5,000–6,000 m (Glud et al., 2013, 2021; Luo et al., 2019; Wenzhöfer et al., 2016). These observations imply that deposited organic materials in trenches do not only consist of resilient pre-aged organic material but also include relatively labile and nutritious organics that can sustain highly active microbial communities thriving at extreme hydrostatic pressure. Indeed, high but variable concentrations of phytodetrital material has been found in hadal sediments (Glud et al., 2013; Wenzhöfer et al., 2016) and deposition in hadal environments appears to be modulated by several processes.

Tidal fluid dynamics may induce internal waves which combined with complex seafloor bathymetry have been suggested to focus (and winnow) relatively fresh material along trench axes (Turnewitsch et al., 2014; van Haren, 2020). This focusing/winnowing of deposited organic material would partly explain the extensive spatial variability in microbial activity encountered along trench axes despite relatively similar surface ocean production (Glud et al., 2021). The material focusing may be further enhanced by more or less continuous gravity driven down-slope transport in near bed nepheloid layers (Itou et al., 2000; Kawagucci et al., 2012; Noguchi et al., 2011).

Hadal trenches are located at plate boundaries and are thus exposed to earthquakes that may trigger large scale submarine slides (Kawamura et al., 2012). The events often remobilize and transfer surface sediments toward trench axis. We here refer to these events as mass wasting (Schwestermann et al., 2020). The mass-wasting events form distinct deposits known as turbidites with relatively stable values of radionuclides such as $^{210}Pb_{ex}$ reflecting the large sudden deposition events (Bao et al., 2018; Ikehara et al., 2016; Luo et al., 2019; McHugh et al., 2016, 2020; Oguri et al., 2013; Usami et al., 2018). Material sorting, reoccurring deposition-loops, sediment compaction, and complex mixing of different sediment sources during an event is, however, expected to result in some variability around the mean $^{210}Pb_{ex}$ concentration in a deposit. The redeposited sediment layers are often associated with abnormal distribution of organic material where older deposits overlay younger material (Bao et al., 2018; Ikehara et al., 2020; Schwestermann et al., 2021; Usami et al., 2021; Xu et al., 2021). However, such events may not only redeposit relic or refractory organic carbon from the slopes toward the trench axes (Kioka et al., 2019a) but may also carry, and focus, relatively fresh phytodetrital material (Oguri et al., 2013) and carrion killed during these catastrophic events (Arai et al., 2013; Oguri et al., 2013). Seismic activity has also been observed to mix and homogenize the relatively fluid sediment surface layers with high porewater contents (Ikehara et al., 2021; Oguri et al., 2016). Bioturbation by fauna is another important process that can contribute to sediment mixing. This process is particularly prominent in fauna rich coastal sediments where surface layers down to 5–10 cm are often characterized by constant $^{210}Pb_{ex}$ and organic carbon values (DeMaster et al., 1985; Glud et al., 1998; McKee et al., 1983; Nittrouer et al., 1984).

Sedimentation rate (SR), mass accumulation rate (MAR) and distribution of organic carbon are the key for resolving benthic mineralization efficacy and carbon sequestration rates, but most investigations have focused on shallow environments. Recent investigations suggest that hadal trenches might be quantitatively important sites for sequestration of organic carbon (Bao et al., 2018; Xu et al., 2021; Zhang et al., 2022), but trench systems remain grossly under sampled and the extent that deposited organic material is retained in the sedimentary record or mineralized remain poorly constrained (Glud et al., 2021; Thamdrup et al., 2021).

In this paper, we quantify deposition dynamics for the past ~150 years' in four different hadal trench systems from the distribution of radionuclides ($^{210}Pb_{ex}$, ^{137}Cs, and ^{14}C) in recovered sediment cores. The study areas underlie oceanic provinces of highly different surface ocean production—from the eutrophic Atacama and Kuril-Kamchatka trenches to the mesotrophic Kermadec Trench, and the oligotrophic Mariana Trench. While surface sediment layers occasionally appeared mixed, presumably due to bioturbation by the activities of epifauna (Weston & Jamieson, 2022; Wolff, 1970) or by earthquake shaking (Ikehara et al., 2021), subsurface sediment

sections appeared laminated and generally exhibited mono-exponential declines of the $^{210}Pb_{ex}$ concentrations. Sedimentation rates derived from radionuclide profiles and organic carbon measurements are used to quantitatively assess hadal deposition dynamics and discuss the importance of carbon sequestration in hadal trench systems.

2. Methods

2.1. Sediment Sampling and Storage

Sediment cores within the four targeted trench systems (Figure 1a), were collected during the cruises of R/V Sonne (Atacama Trench, SO261 from 2 March to 2 April 2018; Figure 1b), R/V Sonne (Kuril-Kamchatka Trench, SO250 from 16 August to 26 September 2016; Figure 1c), R/V Tangaroa (Kermadec Trench, TAN1711 from 24 November to 14 December 2017; Figure 1d), and R/V Yokosuka (Mariana Trench, YK10-16 from 20 November to 4 December 2010; Figure 1e). In total 13 cores were recovered from the trench axes, 3 cores from the abyssal plain, and 2 cores from the abyssal or bathyal slopes. Summary information on the sampling sites is provided in Table 1. Most sediment cores were collected with a multi-corer (Barnett et al., 1984), one site was sampled with a box-corer and three sites were sampled by an autonomous sediment coring lander (Table 1). The sediment cores were quickly transferred to a thermo-regulated room maintaining temperature close to in situ conditions. Within 24 hr, the cores were sectioned, and each sediment slice was homogenized and kept frozen in plastic bags until analysis. In the onshore laboratory wet re-homogenized sediment was transferred to a plastic cube of known internal volume and weight (7.0 cm^3, 4.16 g). The sediment weight was determined before and after drying the samples for a total of 48 hr at 80°C to determine the water content and the dry bulk density. Subsequently the material was ground into powder with an agate mortar and pestle in preparation for measurements of the concentration of the targeted radionuclides.

2.2. Measurements of $^{210}Pb_{ex}$ and ^{137}Cs Concentrations and Calculations of Sedimentation and Mass Accumulation Rates

The distribution of $^{210}Pb_{ex}$ is widely used for resolving recent sediment deposition dynamics. The particle reactive $^{210}Pb_{ex}$ is produced from decay of ^{222}Rn in the atmosphere and the water column, and the nuclide deposits at the sediment surface via particle scavenging (Craig et al., 1972; Koide et al., 1972). Non-bioturbated sediments characterized by slow and steady accumulations exhibit $^{210}Pb_{ex}$ profiles with a mono-exponential decline from the surface layer, and SR and MAR are calculated from this profile. Sediment mixing as induced by bioturbation will reduce the attenuation and maybe even result in vertically relatively stable $^{210}Pb_{ex}$ concentrations (Benninger et al., 1979; DeMaster et al., 1985; Harden et al., 1992; Nittrouer et al., 1984). Without correction for any potential biological sediment mixing, SR and MAR will be correspondingly overestimated. Below we argue (see Section 4.1 in Discussion) for very limited to negligible bioturbation in subsurface hadal sediments, but as we cannot disprove potential contributions from bioturbation, SR and MAR should be regarded as apparent values. Typically, ^{210}Pb investigations are considered to cover a period of 5 half-lives (~110 years), however, the settings of this study were characterized by relatively high $^{210}Pb_{ex}$ concentrations which enabled investigations on deposition dynamics for more extended periods. Considering surface concentrations that were higher than 1.5 Bq g^{-1} and our detection level of ~0.01 Bq g^{-1}, the period of investigation includes at least 7 half-lives of the ^{210}Pb, corresponding to ~150 years. In addition, ^{137}Cs (half-life of 30 years) originating from the past nuclear weapon tests in the Northern Hemisphere and catastrophic accidents at nuclear power plants, was applied as another chronological indicator for recent (after 1955, and the peak fallout of 1963) sediment deposition dynamics (e.g., Fuller et al., 1999; Hirose et al., 2008; Kusakabe et al., 2017).

The analyses of $^{210}Pb_{ex}$ and ^{137}Cs in sediment samples from Atacama, Kermadec and Mariana trenches were carried out at Japan Agency for Marine-Earth Science and Technology (JAMSTEC), while samples from Kuril-Kamchatka Trench were analyzed at The Scottish Universities Environmental Research Centre (SUERC). At both institutions, the radionuclide concentrations were quantified by gamma-ray spectrometry. For five sites in the Atacama Trenches (A1, A2, A4, A5, and A6), the $^{210}Pb_{ex}$ profiles were also quantified in parallel at the Edith Cowan University (ECU, Australia).

At JAMSTEC, 2.0 g of dried sediment powder was placed in a sealed plastic vessel and kept for at least 2 months to establish secular equilibrium between ^{226}Ra and ^{222}Rn. For gamma-ray counting, well-type High-Purity
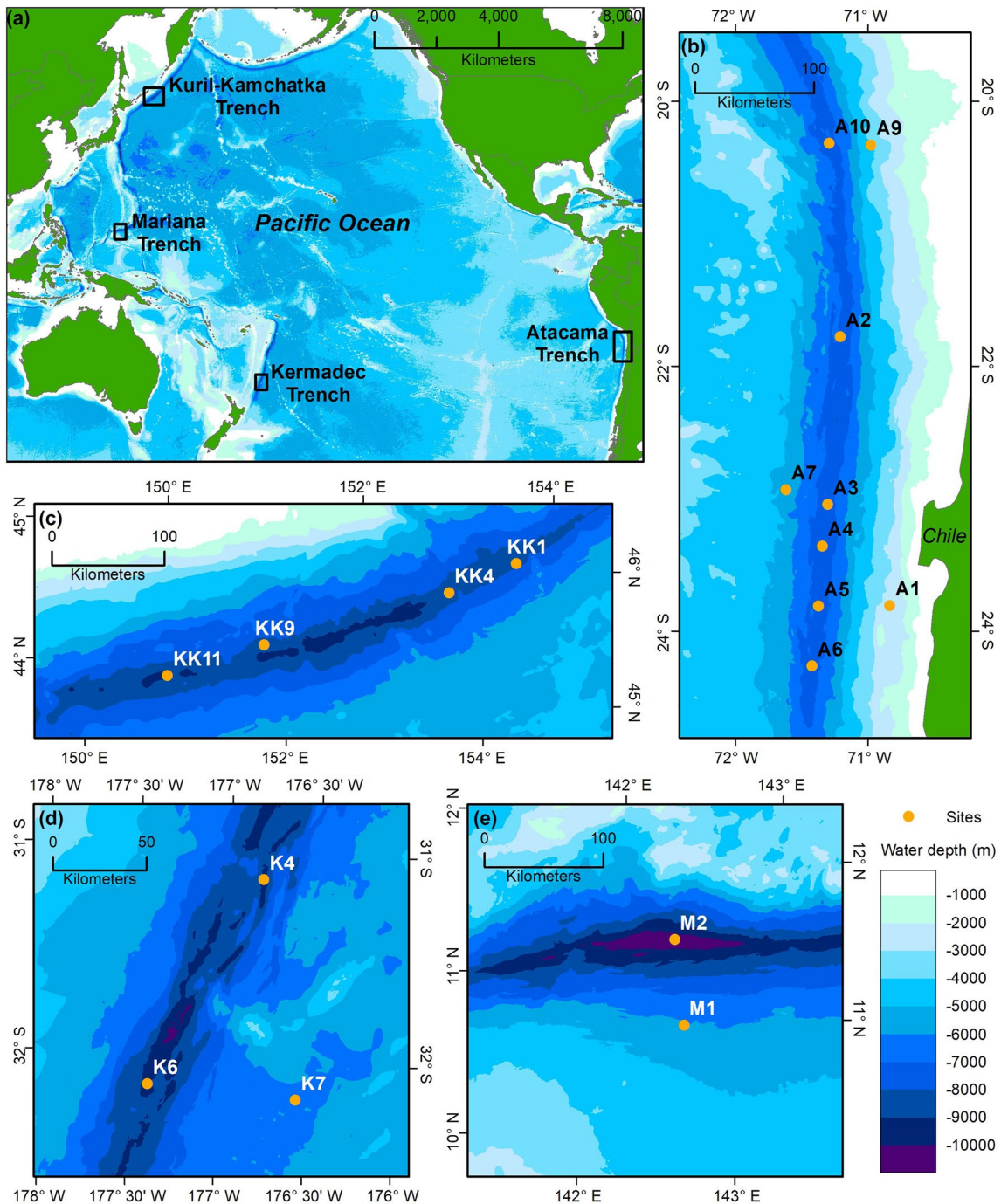
Figure 1. (a) Location of the four targeted trench systems: Atacama, Kuril-Kamchatka, Kermadec and Mariana trenches. Sampling sites in the individual trench regions are depicted in the subpanels; (b) Atacama, (c) Kuril-Kamchatka, (d) Kermadec, and (e) Mariana. All elevation data sourced from the GEBCO Bathymetric Compilation Group (2021). Copyright British Geological Survey © UKRI 2022.

Germanium (HPGe) detectors (GWL120230 or GWL120-15, ORTEC-Ametek) were used. Samples were counted for 1–4 days. The emission peaks of ^{210}Pb, ^{214}Pb, and ^{137}Cs used for the analysis were 46.5, 351.9, and 661.6 keV, respectively. The ^{210}Pb$_{ex}$ concentrations were calculated by subtracting the ^{214}Pb concentrations (as supported ^{210}Pb) from the total ^{210}Pb on the assumption of secular equilibrium between ^{226}Ra and the daughters' nuclides. In case two-standard deviations of the mean ^{210}Pb$_{ex}$ reached negative values, the mean was considered below background and removed from the data set.

Table 1
Sampling Sites, Water Depth, Latitude, Longitude, Core Length, and Sampling Equipment

Trench system	Setting	Site	Net primary productivity (gC m^{-2} y^{-1})	Water depth (m)	Latitude	Longitude	Core length (cm)	Sampling equipment
Atacama	Bathyal continental slope	A1	449	2,560	23° 48.72′S	70° 50.04′W	20	MUC
	Abyssal slope	A9	342	4,050	20° 19.97′S	70° 58.70′W	18	MUC
	Abyssal plain	A7	308	5,500	22° 56.22′S	71° 37.08′W	24	MUC
	Hadal trench axis	A10	306	7,770	20° 19.14′S	71° 17.46′W	38	MUC
	Hadal trench axis	A2	306	7,995	21° 46.86′S	71° 12.48′W	24	MUC
	Hadal trench axis	A3	341	7,915	23° 02.94′S	71° 18.12′W	26	MUC
	Hadal trench axis	A4	335	8,085	23° 21.78′S	71° 20.60′W	34	MUC
	Hadal trench axis	A5	341	7,770	23° 49.02′S	71° 22.32′W	16	MUC
	Hadal trench axis	A6	309	7,720	24° 15.96′S	71° 25.38′W	22	MUC
Kuril-Kamchatka	Hadal trench axis	KK1	215	8,255	45° 50.88′ N	153° 48.00′ E	16	MUC
	Hadal trench axis	KK4	247	8,941	45° 28.75′N	153° 11.65′E	42	MUC
	Hadal trench axis	KK9	215	8,221	44° 39.88′N	151° 28.11′E	12	MUC
	Hadal trench axis	KK11	249	9,540	44° 12.39′N	150° 36.01′E	27	MUC
Kermadec	Abyssal plain	K7	148	6,080	32° 11.22′S	176° 33.66′W	24	BC
	Hadal trench axis	K4	143	9,300	31° 08.41′ S	176° 48.48′ W	15	Lander
	Hadal trench axis	K6	152	9,555	32° 08.93′S	177° 23.91′W	30	MUC
Mariana	Abyssal plain	M1	50.4	6,032	10° 50.33′N	142° 33.69′E	25	Lander
	Hadal trench axis	M2	50.4	10,850	11° 21.94′N	142° 25.68′E	48	Lander

Note. MUC: multi-corer, and BC: box-corer. Net primary productivity was derived from a model of Behrenfeld and Falkowski (1997) and remote sensing data from the period 2009–2018 at the respective sites. The values of Atacama, Kermadec, and Mariana trenches have previously been presented in Glud et al. (2021). Precise depth, latitude, longitude may be slightly varied by correction from the ship positioning. For detail, please contact the author.

At ECU, the ^{210}Pb concentrations were determined through the analysis of the concentration of its granddaughter ^{210}Po by alpha-spectroscopy, assuming secular equilibrium of both radionuclides at the time of analysis (Sanchez-Cabeza et al., 1998). Each sample was spiked with ^{209}Po, and this was followed by a total acid digestion using an analytical microwave, and polonium isotopes were subsequently plated on silver discs. Alpha emissions were quantified using Passivated Implanted Planar Silicon (PIPS) detectors (Model PD-450.18 a.m., Canberra) with a Maestro™ data acquisition software. Some samples from each core were measured by gamma spectrometry to quantify the specific concentrations of ^{226}Ra through the emission lines of its decay product ^{214}Pb (295.2 and 351.9 keV) using calibrated geometries in a HPGe detector (Model SAGe Well, Canberra). The weight of the dried samples used for the gamma-ray analysis ranged from 1 to 6 g. The analysis at ECU and JAMSTEC were conducted on separate cores sampled in the same multi-corer casts, and thus recovered from within 1 m distance of each other on the seabed.

At SUERC, 5.5–20.6 g of dried sediment powders were pressed (10–12 tons of pressure applied using an Enerpac hydraulic disc press) into uniform geometries and the pellets placed into a 55 mm diameter petri dish and sealed with epoxy resin. The sealed samples were then stored for a minimum of 3 weeks before counting to ensure equilibrium between ^{226}Ra and ^{222}Rn. Measurements were made using a low background Profile series HPGe Coaxial photon detector (GEM-S-XLB-C, ORTEC-Ametek). Analysis times ranged between 1 and 9 days. Concentrations of the samples were calculated relative to background measurements and the standard materials in the same geometry to correct for geometry and self-absorption.

MAR (in g cm^{-2} y^{-1}) during periods without any distinct mass-wasting events were estimated based on the Constant Flux:Constant Sedimentation (CF:CS) model (Krishnaswami et al., 1971). Both MAR and SR (in mm y^{-1}) were calculated from sections of the ^{210}Pb$_{ex}$ profiles indicating mono-exponential declines. Depositions during mass wasting were identified by relatively stable ^{210}Pb$_{ex}$ concentrations across more than three subsequent depth intervals and was often associated with clear excursions on the total organic carbon (TOC)

profiles. Depositions formed during mass-wasting events can be associated with shifts in grain size, sorting of settling particles, compaction, or complex mixing of different sediment sources that could result in variations around the mean $^{210}Pb_{ex}$ concentrations of given turbidities. However, layers deposited during mass wasting and being thinner than the resolution of our core sectioning scheme, might have been missed. Our assessments are thus conservative and might underestimate the actual frequency and contributions of mass-wasting events. In this study, relatively stable $^{210}Pb_{ex}$ concentration layers at the sediment surface are not considered to have been formed by mass-wasting events, as bioturbation could have affected the resolved profiles—and contributions from mass-wasting events can thus be regarded as conservative estimates. The average annual mass deposited during mass-wasting events (MAR_{mw}) were calculated as $MAR_{mw} = (\rho\ z)/t$, where ρ is the sediment dry bulk density (g cm^{-3}), z is the horizontal thickness of the target deposited layer (cm) and t is the time of the period considered (~150 years). The total mass accumulation rate thus equaled $MAR_{tot} = MAR + MAR_{mw}$. In cases when more deposits formed by mass-wasting events were identified, their respective contributions were included and averaged into the targeted ~150 years period. The year for a given mass-wasting event was derived from the $^{210}Pb_{ex}$ concentrations at the sediment surface and the concentrations of the layer just above the layer of an identified mass-wasting event.

2.3. Calculation of Pelagic Focusing Factors

To independently assess material focusing along the trench axes, we derived a focusing factor, expressing the ratio between the $^{210}Pb_{ex}$ inventory in the sediment and the calculated pelagic deficit of the ^{210}Pb inventory in the water column (Bacon, 2005; Francois et al., 2004; Kato et al., 2003; Turnewitsch et al., 2004). Assuming steady state, no horizontal material transport and no addition of $^{210}Pb_{ex}$ from subsurface sediment layers, the ^{210}Pb deficient of the pelagic inventory should be equivalent to the $^{210}Pb_{ex}$ inventory and the corresponding focusing factor would thus amount to 1.0. Values above 1.0 or below 1.0 would suggest focusing or winnowing of material, respectively. The $^{210}Pb_{ex}$ inventory in sediments were calculated from the following equation:

$$I = \sum A \cdot z \cdot \mathrm{DBD} \tag{1}$$

where $I = {}^{210}Pb_{ex}$ inventory (Bq cm^{-2}), $A = {}^{210}Pb_{ex}$ concentration (Bq g^{-1}) in the targeted sediment horizon of thickness z (cm) and DBD = dry bulk density of the sediment (grams of dry sediment per cm^3 of wet sediment) at z. In this study, we derived two values for the $^{210}Pb_{ex}$ inventories, either including (MAR_{tot}) or excluding the sediment layers considered to have been deposited during mass-wasting events (MAR). Sediment cores collected at the abyssal plain sites (A7 and K7) contained manganese nodules. Manganese nodules are known to elevate $^{210}Pb_{ex}$ concentration in the upper sediment layers by the release of ^{222}Rn (DeMaster & Cochran, 1982). Therefore, the $^{210}Pb_{ex}$ inventories for these sites were derived from the mono-exponential decline until reaching low background levels assuming a general profile offset as proposed by DeMaster and Cochran (1982). Manganese nodules are frequently encountered both at the sediment-water interface and within sediments (e.g., Jeong et al., 1996). The reason of the distribution is unclear but is related to long term tectonic activity and sediment sieving (Pattan & Parthiban, 2007).

Deficits of ^{210}Pb inventory in the pelagic realm were calculated by subtracting the ^{210}Pb inventory from the ^{226}Ra inventory in the water column. The pelagic inventories of both nuclides were obtained from profiles measured by previous studies at sites close to our benthic sites (Chung & Craig, 1973, 1980, 1983; Thomson & Turekian, 1976). The positions of these sites and the distance between pelagic and benthic sites ranged between 410 and 2,600 km (Table S1). The ^{210}Pb and ^{226}Ra concentrations below the maximal measuring depth were extrapolated to the sea floor assuming constant concentrations (Turnewitsch et al., 2014).

2.4. Measurement of Total Organic Carbon (TOC) Content and Organic Carbon Deposition Rates (OCDR)

The TOC content of Atacama, Kermadec and Mariana trench samples were measured at University of Southern Denmark (SDU), and Kuril-Kamchatka Trench samples were measured at the Scottish Association for Marine Science (SAMS), respectively. At SDU, sediment samples were first acidified, dried and milled. Then these samples were placed in small tin capsules that were transferred to an elemental analyzer (Delta V Advantage, Thermo Scientific). TOC content was derived from parallel sediment cores collected during the same multi-corer

cast. At SAMS, sediment samples were dried and milled after decalcification with 5% sulfuric acid. The processed samples were enclosed in tin capsules, and the contents were measured with an elemental analyzer (Elemental Combustion ECS4010, Costech). To estimate the analytical precision, triplicates of every 5–10th sample were measured. Accuracy of analysis was confirmed by measuring a standard material "medium organic content soil" OAS (B2178, BN 217409, with 3.19% ± 0.07 C and 0.27% ± 0.02 N) in triplicate, prepared in the same way as samples with unknown organic carbon content. Average annual OCDR were calculated from the MAR and the measured TOC content at the sediment surface. The ~150 years averaged OCDR including mass-wasting event layers ($OCDR_{tot}$) were calculated with MAR_{tot} and the TOC content in the respective mass-wasting layers if higher than the TOC content at the sediment surface.

2.5. Determination of ^{14}C Age of Organic Carbon in Sediment From the Mariana Trench

To better constrain of the deposition dynamics inferred by the $^{210}Pb_{ex}$ for profiles in the Mariana trench region, we complemented insight by using available information on the ^{14}C age of bulk organic carbon (e.g., Bao et al., 2018). We measured the ^{14}C ages of bulk organic carbon from Mariana Trench sediments with accelerator mass spectrometer at the National Ocean Sciences Accelerator Mass Spectrometry (NOSAMS), Woods Hole Oceanographic Institution. Prior to the sample preparation, acid treatment was applied to remove residual calcium carbonate. Sample sediment was combusted and purified to CO_2 gas. The CO_2 gas was reduced into graphite and pressed into a sample target holder. Further information of the sample preparation, measurement, and the procedures for ^{14}C age calculation are available at the NOSAMS website (https://www.whoi.edu/nosams/). The obtained conventional ^{14}C ages (Stuiver & Polach, 1977) were converted into calibrated ^{14}C ages (notated as cal y.B.P.) based on the half-life of 5,730 years and the present age at A.D. 1950 according to Reimer et al. (2020) using the Marine20 calibration curve (Heaton et al., 2020). The conversion was carried out using R software and IntCal version 0.3.1 package (developed by Maarten Blaauw, https://cran.r-project.org/web/packages/IntCal/index.html). We used the marine radiocarbon reservoir age of the Marine20 database (http://calib.org/marine/) for samples collected at the Guam and Palau islands (Athens, 1986; Clark et al., 2006; Southon et al., 2016).

2.6. Sediment Photographs

Unfortunately, only a subset of sediment cores collected in the Atacama Trench (A4, A5, and A10) were investigated by this approach. Cores were vertically split and photographed in a laboratory at the Center for Marine Environmental Sciences, University of Bremen (MARUM) by using a Multi-Sensor Core Logger (MSCL; GEOTEK®) equipped with a line scan camera for high-resolution core image acquisition (Figure S1 in Supporting Information S1). These cores were collected in the same multi-corer cast with the cores used for the radionuclide analysis. Onboard photographs of split cores collected at KK1, KK4, KK9, and KK11 were obtained from the A.V. Zhirmunsky National Scientific Center of Marine Biology and V.I. Il'ichev Pacific Oceanological Institute, and these unpublished images are included in the (Figure S2 in Supporting Information S1). Two of the sites collected in the Kermadec Trench region (K4 and K7) had cores available to be vertically split and photographed using a MSCL at University of Otago equipped with a line scan camera for high-resolution core image acquisition (Figure S3 in Supporting Information S1).

3. Results

Below we present the results of the radionuclide and TOC measurements for all sites in the investigated trench systems. More specific comments on the respective profiles, available photographs of split sediment cores and linear scale $^{210}Pb_{ex}$ plots are presented in the Supporting Information S2 and Figures S1 to S5 in Supporting Information S1.

3.1. Sediment Profiles of $^{210}Pb_{ex}$ and TOC in the Eutrophic Atacama Trench System

Nine sites were targeted in the Atacama Trench region: one at the bathyal continental slope (A1), one at the abyssal slope (A9), one at an abyssal plain site (A7), and six along the trench axis (A10, A2, A3, A4, A5, and A6) (Figures 1a and 1b, Table 1; Table S2). At five sites (A1, A2, A4, A5, and A6), $^{210}Pb_{ex}$ profiles were derived from two separate sediment cores recovered in the same multi-corer cast and analyzed by two different

procedures and in two different laboratories (for details, see Section 2.2 in Materials and Methods). Except for slight misalignments of the sediment surface at A1, A2, and A5, the two approaches provided very similar results and gave confidence in the derived values (Figure 2 and Table 2). As expected, no ^{137}Cs was detected in any Atacama Trench sediments due to low ^{137}Cs supply in the Southern Hemisphere (Aoyama et al., 2006; Tsumune et al., 2011). At the bathyal site (A1), and the abyssal plain site (A7), the $^{210}Pb_{ex}$ profiles presented mono-exponential declines from the surface to a sediment depth of approximately 10 cm (Figure 2). The TOC content at these two sites declined gradually with sediment depth, but with much higher values (2.32% at 0–1 cm depth) at the bathyal site (A1) as compared to the abyssal plain site (A7) (0.67% at 0–1 cm depth).

The abyssal slope site, A9, is located close to the edge of the trench and exhibited a mixed sediment surface with variable $^{210}Pb_{ex}$ concentrations varying between 0.54 and 0.16 Bq g^{-1} in the interval from 0 to 6 cm depth. From these depths, values decline exponentially (Figure 2). Similarly, the TOC content within the upper 4 cm appears constant, and thereafter TOC gradually increased with depth (Figure 2). The mixed surface could be the result of bioturbation or a recent mass wasting with material of a distinctly different TOC signature. However, we cannot discriminate between these factors and the surface layer is not considered to be the result of mass wasting during the further interpretations.

The hadal site A10, located 30 km west of A9, also showed a sediment profile with almost constant $^{210}Pb_{ex}$ concentrations in the surface layer, from the surface to 3 cm depth. The mixed surface layer was followed by an exponential decline in concentration down to undetectable levels at 10 cm. The average TOC content was 1.05% at 0–3 cm, which is distinctly lower than peak values encountered at 4–5 cm of depth (Figure 2). At A2, the $^{210}Pb_{ex}$ concentrations and the TOC content declined from the surface to 5 cm depth. Hereafter the $^{210}Pb_{ex}$ concentrations remained relatively stable until 12.5 cm depth, the depth interval was associated with an abnormal peak in the TOC content. The profiles suggest that the layer is formed by a mass-wasting deposit. The depositional age, based on the $^{210}Pb_{ex}$ concentrations is calculated to be more than ~90 years old (Table S3 in Supporting Information S2). At A3, surface layers appeared mixed with relatively stable $^{210}Pb_{ex}$ concentrations and TOC values. But at 5 cm depth the $^{210}Pb_{ex}$ begins decreasing exponentially along with a gradual decline in TOC. At A4, the $^{210}Pb_{ex}$ concentrations decline exponentially but relatively stable concentrations were encountered in the depth interval from 7 to 10 cm depth. This layer was followed by another exponential decline in $^{210}Pb_{ex}$ concentrations. The TOC content expressed an anomaly at 10–15 cm. The offset in the depth of the observed anomalies in TOC and $^{210}Pb_{ex}$ concentrations could be related to the fact that analyses were done on parallel cores. Following the definitions that were outlined above (Section 2.2) we ascribe these depositions to a mass-wasting event. The deposition age of this layer is more than ~90 years old (Table S3 in Supporting Information S2).

At A5, the surface layer appeared to be mixed down to 3–4 cm and subsequently the $^{210}Pb_{ex}$ concentrations followed an exponential decline down to 10 cm depth. Here values remained relatively stable for $^{210}Pb_{ex}$ until 15 cm depth. The layer appears to have been formed by a mass-wasting event more than ~130–140 years old. A6 exhibited a steady decrease in $^{210}Pb_{ex}$ concentration from the surface until reaching background levels in the deepest sampled layer, suggesting no mixing or mass-wasting deposits at this site during the past ~150 years.

Excluding any contributions from mass-wasting deposits, the SR and MAR during steady deposition periods (as derived from sections of exponential declining $^{210}Pb_{ex}$ concentrations) amounted to 0.53–0.74 mm y^{-1} (0.028–0.037 g cm^{-2} y^{-1}) for the bathyal slope site (A1), 0.33 mm y^{-1} (0.018 g cm^{-2} y^{-1}) for the abyssal slope site (A9), 0.65 mm y^{-1} (0.024 g cm^{-2} y^{-1}) for the abyssal plain site (A7), and 0.29–0.79 mm y^{-1} (0.012–0.093 g cm^{-2} y^{-1}) for the hadal sites along the trench axis (Table 2). Contributions from infrequent mass-wasting events contributed average Mass Accumulation Rates (MAR$_{mw}$) of 0.013–0.033 g cm^{-2} y^{-1}.

3.2. Sediment Profiles of $^{210}Pb_{ex}$, ^{137}Cs and TOC in the Eutrophic Kuril-Kamchatka Trench System

Four hadal sites were targeted in the Kuril-Kamchatka Trench system (Figures 1a, 1c, and 3a and Table S2). Unlike Atacama Trench sediments, ^{137}Cs was detected in all sediment cores, but unfortunately, no TOC data are available from KK1 and KK4. The $^{210}Pb_{ex}$ concentrations at KK1 showed a mono-exponential decline from the sediment surface to 16 cm depth. The sediment core showed a laminated structure, and the general lack of deep burrowing, hadal infauna (discussed in the Section 4.1) suggest that the $^{210}Pb_{ex}$ profile is the result of a constant deposition and has no signatures of mass-wasting events. The ^{137}Cs penetrated from the surface to 4 cm depth in this core, confirming that these layers were affected by the nuclide deposited after 1955, when [137]Cs
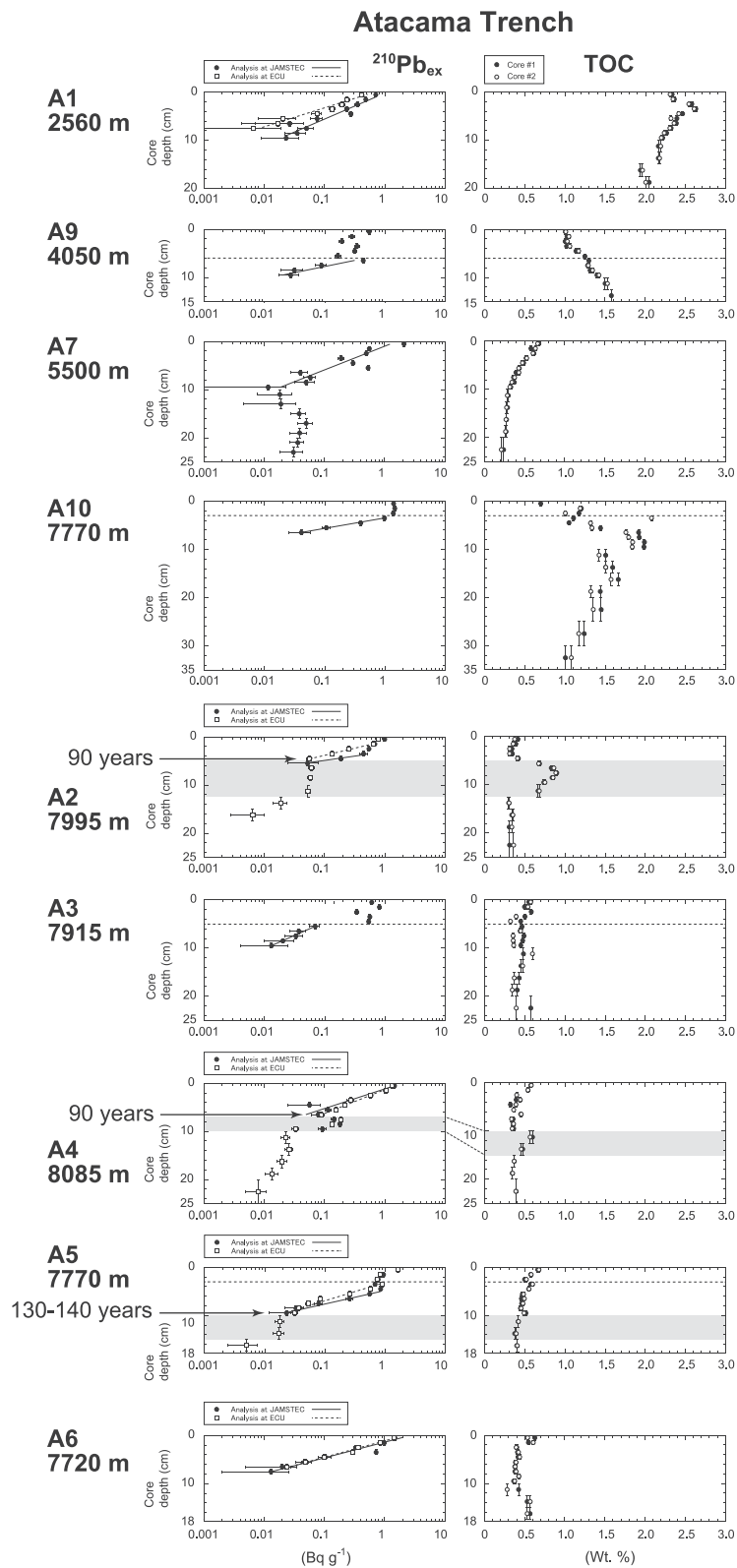
Figure 2.

Table 2

Sedimentation Rate (SR), Mass Accumulation Rate (MAR), Depth Applied for Calculating SR and MAR, Total Organic Content (TOC) in the Surface (0–1 cm Depth), Organic Carbon Deposition Rate (OCDR), as Well as Mass Accumulation Rate Mediated Mass-Wasting Events (MAR$_{mw}$), and Total Mass Accumulation Rate (MAR$_{tot}$) in the Four Trench Systems

Trench	Site	SR (mm y^{-1})	MAR (g cm^{-2} y^{-1})	Applied interval (cm)	TOC (%)[a]	OCDR (gC m^{-2} y^{-1})	MAR$_{mw}$ (g cm^{-2} y^{-1})[b]	MAR$_{tot}$ (g cm^{-2} y^{-1})
Atacama	A1	0.74	0.037	0.5–9.5	2.32	8.6	–	–
	A1-E	0.53	0.028	0.5–7.5	2.32	6.4	–	–
	A9	0.33	0.018	6.5–9.5	1.01	1.8	–	–
	A7	0.65	0.024	0.5–9.5	0.67	1.6	–	–
	A10	0.29	0.012	2.5–6.5	0.94	1.2	–	–
	A2	0.29	0.028	3.5–5.5	0.39	1.1	–	–
	A2-E	0.45	0.042	0.5–4.5	0.39	1.6	0.033	0.07
	A3	0.79	0.093	5.5–9.5	0.57	5.3	–	–
	A4	0.56	0.055	0.5–6.5	0.58	3.2	0.015	0.07
	A4-E	0.67	0.062	0.5–6.5	0.58	3.6	0.013	0.08
	A5	0.39	0.027	4.5–9.5	0.67	1.8	–	–
	A5-E	0.51	0.041	3.5–9.5	0.67	2.7	0.027	0.07
	A6	0.43	0.032	0.5–7.5	0.58	1.8	–	–
	A6-E	0.45	0.043	0.5–6.5	0.58	2.5	–	–
Kuril-Kamchatka	KK1	0.80	0.036	0.5–15	no data	–	–	–
	KK4	1.79	0.082	9.5–19	no data	–	0.055	0.14
	KK9	0.28	0.012	2.5–7.5	1.04	1.2	–	–
	KK11[c]	0.89	0.029	2.5–4.5	1.08	3.1	0.020	0.05
	KK11[d]	0.49	0.028	15–23	0.93[e]	2.6	0.020	0.05
Kermadec	K7	0.31	0.020	0.5–3.5	0.37	0.7	–	–
	K4	0.30	0.015	0.5–3.5	0.45	0.7	0.040	0.05
	K6	0.39	0.029	0.5–7.0	0.43	1.3	–	–
Mariana	M1	–	–	–	0.49	–	–	–
	M2	0.39[f]	0.044[f]	0.5–6.5	0.43	1.9	0.125	0.17

Note. Suffix -E indicate that the ^{210}Pb$_{ex}$ concentrations were measured at Edith Cowan University. The other Atacama Trench samples were measured at Japan Agency for Marine-Earth Science and Technology.

[a]TOC of all Atacama, KK11 and all Kermadec samples are averaged from the two different cores collected in the same casts. [b]~150 years averaged value. [c]Curve A. [d]Curve B (for these curves, see ^{210}Pb$_{ex}$ plot of KK11 in Figure 3a). [e]Averaged value at the 4–6 cm depth. [f]Glud et al. (2013).

fallout was intensified by atmospheric nuclear tests (Hirose et al., 2008). But the fact that the maximum value is encountered at the sediment surface indicate that the layer is a result of a secondary deposition event potentially combined with a downward molecular diffusion of non-sorbed ^{137}Cs (see Section 4.1) or potential bioturbation. At KK4, both the ^{210}Pb$_{ex}$ and ^{137}Cs profiles indicated a mixed surface layer with relatively stable concentration down to 12 cm depth. The mixing could be the result of recent mass-wasting event or intense bioturbation at the surface, but we cannot discriminate between these two factors. From 12 to 20 cm depth, the ^{210}Pb$_{ex}$ profile exhibited a mono-exponential decline, while values in a deeper layer (20–35 cm) remained relatively constant and is presumed to be the result of an unidentified mass-wasting event. The deposition age of this layer is estimated to be more than ~90 years old (Table S3 in Supporting Information S2). The ^{137}Cs concentration below the well-mixed surface layer declined and penetrated an additional 6 cm into the sediment. Again, this pattern can be ascribed to

Figure 2. ^{210}Pb$_{ex}$ concentration and total organic carbon (TOC) profiles measured in sediment cores recovered in the Atacama Trench region. Sediment layers deposited during mass-wasting events, as inferred from relatively stable ^{210}Pb$_{ex}$ concentrations over distinct depth intervals and typically associated with abnormal TOC distributions are shown in gray hatches (see Section 2.2 and Supporting Information S2 for further description). Dashed horizontal lines at A9, A10, A3, and A5 indicate the depth for surface mixed layers. Solid and dashed lines in the ^{210}Pb$_{ex}$ graphs were obtained by exponential curve fitting to the respective ^{210}Pb$_{ex}$ concentration profiles in the indicated depth interval (Table 2).
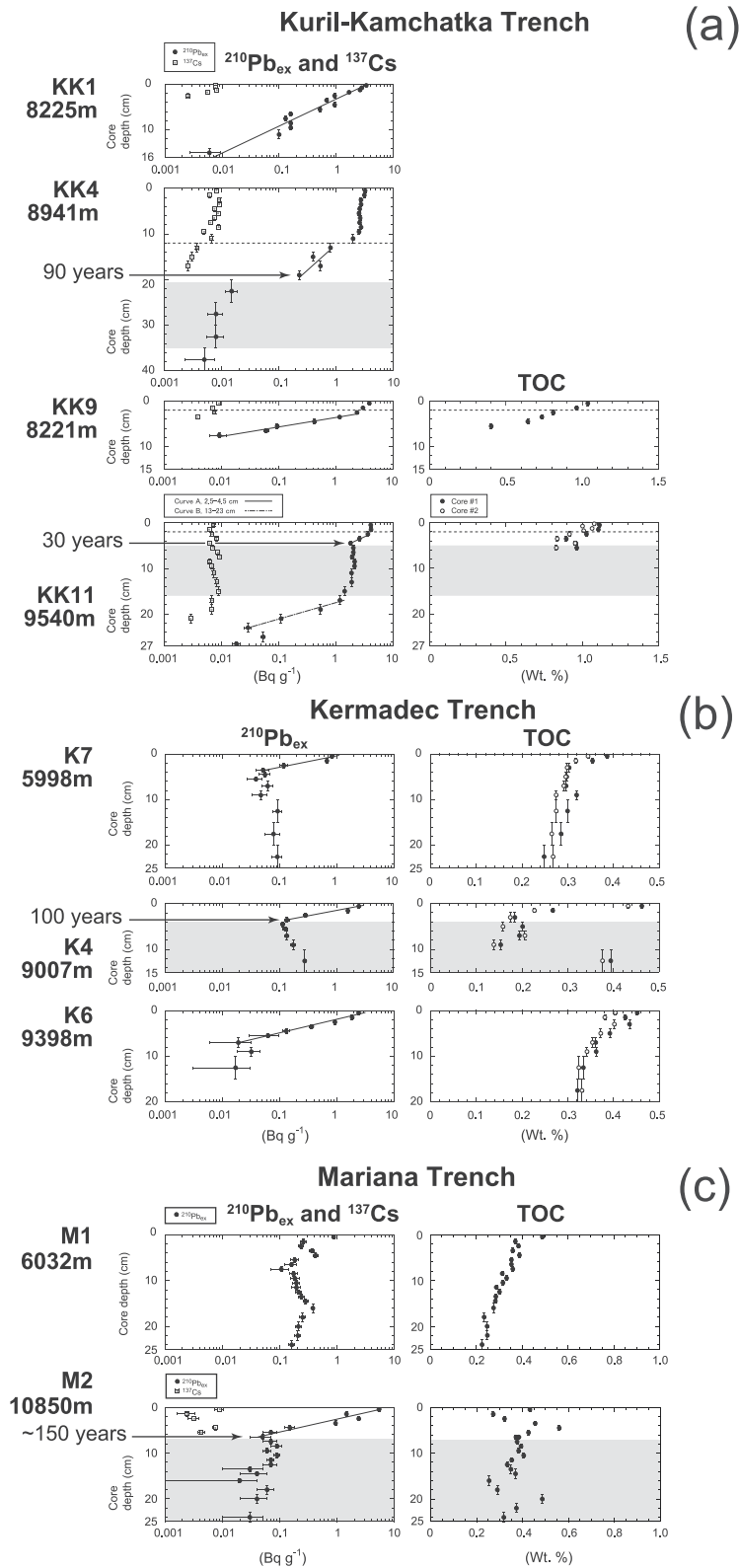
Figure 3. $^{210}Pb_{ex}$, ^{137}Cs, and total organic carbon (TOC) profiles measured in sediment cores recovered from in Kuril-Kamchatka (a), the Kermadec (b) and the Mariana (c) trench systems. Sediment layers deposited during mass-wasting events, as inferred from elevated and relatively constant $^{210}Pb_{ex}$ concentrations over distinct depth intervals (for both trench cores) and abnormal TOC distribution (for Kermadec Trench cores only) are shown in gray hatches. Dashed horizontal lines at KK4, KK9, and KK11 indicate the depth of apparent surface mixing. Solid lines in the plots of $^{210}Pb_{ex}$ profiles were obtained by exponential curve fitting.

a downward molecular diffusion of non-sorbed ^{137}Cs because bioturbation at this depth in the sediment does not seem likely (see also Section 4.1). At KK9, the top 2 cm at the sediment surface seems to be affected by mixing, but ^{210}Pb$_{ex}$ concentration from 3 to 8 cm showed a mono-exponential decline. As for site KK1, ^{137}Cs peaked at the sediment surface and penetrated to 4 cm depth. The TOC showed gradual decline from 1.04% at the surface to 0.40% at the maximum sampling depth. At KK11, the top 2 cm of the sediment appeared mixed, followed by a slight exponential decline and another 11 cm (at 5–16 cm) thick layer with a distinct signature of mass-wasting event with nearly stable ^{210}Pb$_{ex}$ and ^{137}Cs concentrations (Figure 3a and Table S2). The inferred age for the deposition is more than ∼30 years old (Table S3 in Supporting Information S2). The ^{137}Cs penetrated 6 cm into the sediment layer below the mass-wasting event layer presumably due to diffusion because infauna-mediated bioturbation this deep in a hadal sediment seems unlikely (see Section 4.1). The ^{210}Pb$_{ex}$ concentration declined exponentially below the thick mixed layer. TOC content at the surface was 1.1% and declined slightly to ∼0.9% at the maximum depth of analysis (TOC was not analyzed below 6 cm depth).

Excluding the contributions from mass-wasting events, the derived SR and MAR at the four hadal sites in Kuril-Kamchatka Trench were 0.80 mm y^{-1} (0.036 g cm^{-2} y^{-1}) at KK1, 1.26 mm y^{-1} (0.056 g cm^{-2} y^{-1}) at KK4, 0.28 mm y^{-1} (0.012 g cm^{-2} y^{-1}) at KK9, and 0.61–0.89 mm y^{-1} (0.029–0.032 g cm^{-2} y^{-1}) at KK11 (Table 2). Average annual contribution from mass-wasting events across the investigated time window (∼150 years) ranged from 0.020 to 0.055 g cm^{-2} y^{-1}.

3.3. Sediment Profiles of ^{210}Pb$_{ex}$ and TOC in the Mesotrophic Kermadec Trench

Three sites were sampled in the Kermadec Trench (Figures 1a, 1d, and 3b and Table S2): one at a nearby abyssal plain site (K7) and two located at the trench axis (K4 and K6). Like the Atacama Trench, no ^{137}Cs was detected in any of the sampled Kermadec Trench sediment. The ^{210}Pb$_{ex}$ concentration profiles at K7 showed a steep decrease from the surface to a depth of 4 cm, before reaching a stable low level to the bottom of the core (25 cm; Figure 3b). Because ^{214}Pb profile showed gradual increase with depth (Table S2 and Figure S5 in Supporting Information S1), we ascribe the low but persistent ^{210}Pb$_{ex}$ concentration to the release of ^{222}Rn from manganese oxide (DeMaster & Cochran, 1982). Manganese nodules occurred on the sediment surface and were found in the recovered sediment. The TOC content gradually decreased from 0.34% to 0.38% at the sediment surface to 0.25%–0.27% at the core bottom.

At K4, initially, the ^{210}Pb$_{ex}$ concentration declined exponentially down to 5 cm depth, thereafter concentration began to rise to a maximum at the core bottom (16 cm) that also had relatively high TOC levels (0.39%; Figure 3b). While the surface layer could reflect steady sediment accumulation, the deeper layer appears to have been formed by mass wasting from the upper trench slope located west of the trench axis (Ballance et al., 2000). Based on the ^{210}Pb$_{ex}$ concentrations at the sediment surface and the averaged values from the mass-wasting event layer, the deposition of this layer would have occurred older than ∼100 years ago (Table S3 in Supporting Information S2).

At K6, the ^{210}Pb$_{ex}$ concentration declined mono-exponentially from the surface to 8 cm depth. The values in the bottom layer (8–15 cm) appeared relatively stable, but values are low and given the counting accuracy it is not certain that this reflects a mixing or redeposition event. The TOC content decreased gradually from the surface (0.40%–0.45%) down to 20 cm (0.32%–0.33%). The derived SR and MAR rates at the abyssal plain site (K7) amounted to 0.31 mm y^{-1} (0.020 g cm^{-2} y^{-1}) while values at the two hadal sites were 0.30–0.39 mm y^{-1} (0.015–0.029 g cm^{-2} y^{-1}). The average annual contribution to the MAR$_{tot}$ from mass wasting at K4 amounted to 0.040 g cm^{-2} y^{-1} (Table 2).

3.4. Sediment Profiles of ^{210}Pb$_{ex}$, ^{137}Cs, ^{14}C Age of Bulk Organic Carbon and TOC in the Oligotrophic Mariana Trench

Two sediment cores from the Mariana Trench region were investigated (Figures 1a, 1e, and 3c and Table S2): one from an abyssal plain site (M1) and one from the trench axis (M2). The ^{210}Pb$_{ex}$ concentrations and the TOC content from these two sites have previously been presented (Glud et al., 2013) but not been fully interpreted. The ^{210}Pb$_{ex}$ concentrations at M1 were elevated at the surface (0.87 Bq g^{-1}), but values remained relatively low and without any distinct decline with increasing sediment depth (Figure 3c). The ^{214}Pb profile exhibited relatively higher concentration at the sediment surface (0.29–0.37 Bq g^{-1}) that increased down through the sediment (0.42–0.57 Bq g^{-1}) (Figure S5 in Supporting Information S1). As for M1, we ascribe the observations to the occurrence of manganese nodules that were encountered in the sediment and also have been observed previously

in other low latitude Pacific regions (Iijima et al., 2016; Jeong et al., 1996). The observed $^{210}Pb_{ex}$ profile thus appears to be strongly confounded by the release of ^{222}Rn from manganese oxide (DeMaster & Cochran, 1982), and it was not possible to derive any SR and MAR from the data at site M1. We could not detect any ^{137}Cs at this abyssal site. The TOC content decreased from the sediment surface (0.49%) to the core bottom (0.23%). The ^{14}C age of bulk organic carbon expressed a linear decrease from 6,240 cal y.B.P at 4.5 cm depth to 22,220 cal y.B.P. at 24.5 cm. However, due to preferential decomposition of labile organic material and preaging of more refractory organics, it is not easy to derive sedimentation rates from the vertical distribution of bulk organic carbon ^{14}C age in dynamic benthic settings (Ausín et al., 2021; Blair & Aller, 2012; Wang et al., 1996).

The profile of $^{210}Pb_{ex}$ at the hadal site, M2, showed a steep exponential decline from the surface down to 7 cm depth, overlying a layer with relatively low and fluctuating $^{210}Pb_{ex}$ concentrations down to 25 cm. The ^{137}Cs was detected from the surface down to 6 cm depth (Figure 3c). This core also had downward increase of ^{214}Pb (0.06–0.16 Bq g^{-1}), but the concentration was much lower than M1 (Figure S5 in Supporting Information S1). The profile of TOC expressed highly fluctuating values ranging between 0.25% and 0.56%. The ^{14}C age of the bulk organic carbon was 1,710–3,675 cal y.B.P. at the surface, but the age remained relatively stable around 4,415 cal. y.B.P. in the deeper sediment layers (Figure S5in Supporting Information S1). The distribution of $^{210}Pb_{ex}$, TOC and ^{14}C age of bulk organic carbon, suggest that the sediment layer below 7 cm depth has been formed by a mass-wasting event. The deposition age of this layer is estimated to ∼150. The SR and MAR derived from the $^{210}Pb_{ex}$ profile amounted to 0.39 mm y^{-1} and 0.044 g cm^{-2} y^{-1}, respectively (Table 2), while the MAR$_{tot}$ amounted to 0.125 g cm^{-2} y^{-1}.

4. Discussion

4.1. Potential Bioturbation of the Sediments in the Hadal Trench Axes

This study derives estimates for SR, MAR, MAR$_{mw}$, and OCDR in some of the deepest trenches on the earth using measured sediment profiles of $^{210}Pb_{ex}$ and TOC. The interpretations presume that bioturbation of subsurface sediments is negligible and that sections of subsurface sediment expressing mono-exponential decline in $^{210}Pb_{ex}$ concentrations reflect layers of continuous and constant deposition (Glud et al., 1998; McKee et al., 1983; Nittrouer et al., 1984; Nozaki et al., 1977) while sections with relatively stable $^{210}Pb_{ex}$ concentrations are deposited during mass-wasting events which are typically induced by seismic activity. To the extent bioturbation contributes to the shaping of the $^{210}Pb_{ex}$ profiles, the derived MAR and MAR$_{mw}$ might be overestimated (Carpenter et al., 1982; Harden et al., 1992; Nittrouer et al., 1984). Below we argue and provide evidence for why we find it plausible that contribution of bioturbation in subsurface hadal sediments can be ignored and that the derived SR, MAR, and MAR$_{mw}$ values represent robust first-order assessments.

For some hadal sites the surface sediments appeared mixed (Figures 2 and 3). This apparent mixing could be caused by bioturbation, recent mass-wasting events (Arai et al., 2013; McHugh et al., 2016; Oguri et al., 2013) or earthquake-induced surface mixing (Ikehara et al., 2021; Oguri et al., 2016). Hadal environment can have a high abundance of benthic epifauna such as amphipods and holothurians (Gebruk et al., 2020; Jażdżewska, 2015; Weston & Jamieson, 2022; Wolff, 1970) and it is likely that these taxa contribute to sediment surface mixing. Therefore, we refrain from using measurements in mixed surface layers to assess the deposition dynamics or deposition rates. However, hadal infauna communities are dominated by meiobenthos such as nematode and foraminifera that are confined to the sediment surface and larger infauna with the potential for sediment mixing are rare (Danovaro et al., 2002; Kamenev et al., 2022; Leduc & Rowden, 2018; Shimabukuro et al., 2022; Todo et al., 2005). Available data suggest that the oxygen penetration of hadal sediments is surprisingly shallow (Glud et al., 2021). For instance, oxygen only penetrated 2.6–4.1 cm into sediments along the Atacama Trench axis and the subsurface sediments were anoxic (Glud et al., 2021). Meiobenthos was only encountered in the upper few cm from hadal Atacama Trench sediments (Shimabukuro et al., 2022). This contrast to conditions in bioturbated systems; where meiofauna is known to extend much deeper in the sediment as they inhabit the oxic burrows, funnels, and galleries (Koller et al., 2006). During the expedition to Atacama Trench, we recovered and sectioned ∼100 MUC cores from hadal depth for a wide range of analysis. We did not encounter any burrow structures or larger infauna in any cores. Sampling during the expedition to Kermadec Trench was less successful, but still we did not encounter any burrow structures or larger infauna in the 16 sediment cores and the one box core that was retrieved from hadal depth. Previous studies described that the abundance of nematodes attenuated strongly with decreasing sediment depth and were found only in the surface sediments (at 0–3 cm) with a few individuals per cm^{-3} from hadal Kermadec Trench sediment (Leduc & Rowden, 2018). Distributions of benthic organisms in

the hadal Mariana Trench (Challenger Deep) are little reported except for some epifauna (Gallo et al., 2015) and benthic foraminifera (Todo et al., 2005), and the vertical distribution of benthic organisms is unknown. We acknowledge that larger infauna and burrows still could exist in these settings, but we did not observe any despite relatively extensive sampling.

Available photographs of split cores from the Atacama Trench showed distinct laminae structures and no traces of bioturbation (Figure S1 in Supporting Information S1). Unfortunately, we only allocated the three presented cores (from A4, A5, and A10) for photographing, due to a high demand on sediment material during the cruise. We acknowledge that this is a small number of data, but the ones available, are consistent with negligible bioturbation in the subsurface sediment. During the cruise to Kuril-Kamchatka Trench photographs were taken for the four targeted sites and the photographs have kindly been provided by the onboard scientists (see Section 2.6 and Figure S2 in Supporting Information S1). The photographs are less clear, but laminar structures in the subsurface sections remain (Figure S2 in Supporting Information S1), and the images provide no evidence of bioturbation. Sediment photograph taken of the split K4 core from Kermadec Trench also indicated clear laminated structures and mass wasting layers were confined (Figure S3 in Supporting Information S1). We do not have any photographs of split sediment cores from the Mariana Trenches.

In the Kuril-Kamchatka Trench, we found significant levels of ^{137}Cs in the trench axis sediments and two different types of profiles were encountered. At KK1 and KK9, the ^{137}Cs concentration exhibited an absolute maximum at the surface and a gradual decline to the maximum measuring depth at 2 cm. In a scenario with continuous vertical sedimentation (at rates as derived from the respective $^{210}Pb_{ex}$ profile) the maximum contribution of ^{137}Cs should be at 4.3 and 1.5 cm at KK1 and KK4, respectively indicating peak deposition in 1963 (Hirose et al., 2008). Bioturbation cannot explain a maximum ^{137}Cs concentration at the sediment surface, rather the distribution of ^{137}Cs indicate displacements and secondary deposition of sediment from the trench slopes along the trench axes. Even though we cannot exclude a contribution from bioturbation, down core attenuation of ^{137}Cs could also be explained by post-depositional molecular diffusion of non-sorbed ^{137}Cs diffusion (Davis et al., 1984; Klaminder et al., 2012). In contrast to strongly bound ^{210}Pb, desorption dynamics have been shown to affect the distribution of ^{137}Cs in marine sediments even without the presence of bioturbating infauna (Davis et al., 1984; Klaminder et al., 2012; Yokoyama et al., 2022). Assuming an intermediary apparent diffusion coefficient for ^{137}Cs of 1.0×10^{-9} cm^2 sec^{-1} (Table S4 in Supporting Information S2) and an initial concentration of 1.83×10^{-5} pmol of ^{137}Cs in a 1 cm confined sediment layer (equal to 0.01 Bq; and similar to the concentration at the present surface sediment in the hadal Kuril-Kamchatka Trench) and accounting for radioactive decay, we calculated that deposited ^{137}Cs could be displaced by up to 6 cm within a 60-year time period (see Figure S6 in Supporting Information S1) using a non-sorbed molecular diffusion model (Berg et al., 2007). Thus, the ^{137}Cs profiles do not shed light on the extent that bioturbation contributes to radionuclide or sediment mixing at these sites and the profiles could be formed by secondary deposition and molecular diffusion. At KK4 and KK11, relatively stable concentrations of ^{137}Cs and $^{210}Pb_{ex}$ were encountered in the upper 12 and 16 cm, respectively. Profiles that could have been formed by bioturbation or by sediment mixing during secondary deposition event. In the layers below the sections of apparently well-mixed sediment, both radionuclides attenuated exponentially with ^{137}Cs reaching 6 cm into the deeper sections. We are inclined to consider the profiles to be a result of mass-wasting events followed by subsequent downward molecular diffusion of non-sorbed ^{137}Cs. The model results show that diffusion of ^{137}Cs to 2.0–6.0 cm depth within relevant time scales is feasible (Figure S6 and Table S5 in Supporting Information S1). Although the calculation is idealized as initial ^{137}Cs concentration in 1955 and the change of the historical ^{137}Cs input at the hadal environment are unknown, the model suggests that inconsistency between initial deposition age from the ^{137}Cs penetration depth and the SR derived from the benthic $^{210}Pb_{ex}$ attenuation can be explained by the diffusion of ^{137}Cs, even if the sediment layer remain unaffected by bioturbation.

We argue that bioturbation in subsurface hadal sediments is negligible, but we at the same time acknowledge that we cannot fully exclude the influence of bioturbation in these subsurface layers. Consequently, the derived SR, MAR, MAR$_{tot}$, and OCDR in a strict sense should be regarded as apparent values (upper limit for the true value).

4.2. Sedimentation, Focusing and Mass Accumulation Along Trench Axes

To quantitatively assess the potential enhancement of material focusing along the trench axes we derived the focusing factors in the four investigated trench regions. The focusing factors at the three abyssal plain sites adja-

Table 3

$^{210}Pb_{ex}$ Inventories in Abyssal and Hadal Sediments, ^{226}Ra, ^{210}Pb and Deficient $^{210}Pb_{ex}$ Inventories in the Water Column and Focusing Factor

Trench system	Site	Water depth (m)	Net primary productivity (gC m^{-2} y^{-1})	$^{210}Pb_{ex}$ inventory in sediment no or excluding mass-wasting event layer (Bq cm^{-2})		$^{210}Pb_{ex}$ inventory in sediment including mass-wasting event layer (Bq cm^{-2})		^{226}Ra inventory in the water column (Bq cm^{-2})	^{210}Pb inventory in the water column (Bq cm^{-2})	Deficient $^{210}Pb_{ex}$ inventory in the water column (Bq cm^{-2})		Focusing factor no or excluding mass-wasting event layer		Focusing factor including mass-wasting event layer	
Atacama	A9	4,050	342	0.98	(0.09)	–	–	1.42	1.17	0.25	–	4.0	(0.2)	–	–
	A7	5,500	308	1.25	(0.11)	–	–	2.19	1.58	0.61	–	2.0	(0.2)	–	–
	A10	7,770	306	2.16	(0.09)	–	–	3.41	2.22	1.20	–	1.8	(0.1)	–	–
	A2	7,995	306	2.28	(0.23)	–	–	3.53	2.28	1.26	–	1.8	(0.2)	–	–
	A2-E	7,995	306	1.56	(0.11)	1.73	(0.10)	3.53	2.28	1.26	–	1.2	(0.1)	1.4	(0.1)
	A3	7,915	341	2.37	(0.15)	–	–	3.49	2.26	1.23	–	1.9	(0.1)	–	–
	A4	8,085	335	2.17	(0.12)	2.50	(0.15)	3.58	2.30	1.28	–	1.7	(0.1)	2.0	(0.1)
	A4-E	8,085	335	2.73	(0.19)	2.97	(0.20)	3.58	2.30	1.28	–	2.1	(0.2)	2.3	(0.2)
	A5	7,770	341	3.24	(0.15)	–	–	3.41	2.22	1.20	–	2.7	(0.1)	–	–
	A5-E	7,770	341	3.15	(0.19)	3.22	(0.20)	3.41	2.22	1.20	–	2.6	(0.2)	2.7	(0.1)
	A6	7,720	309	2.47	(0.14)	–	–	3.39	2.20	1.18	–	2.1	(0.1)	–	–
	A6-E	7,720	309	2.44	(0.14)	–	–	3.39	2.20	1.18	–	2.1	(0.1)	–	–
Kuril-Kamchatka	KK1	8,225	215	3.00	(0.08)	–	–	4.00	2.26	1.74	–	1.7	(0.01)	–	–
	KK4	8,941	247	11.2	(0.17)	11.3	(0.05)	4.37	2.45	1.92	–	5.8	(0.02)	5.9	(0.03)
	KK9	8,221	215	3.14	(0.14)	–	–	4.00	2.26	1.74	–	1.8	(0.02)	–	–
	KK11	9,540	249	6.41	(0.11)	13.8	(0.06)	4.69	2.62	2.07	–	3.1	(0.02)	6.7	(0.03)
Kermadec	K7	6,080	148	1.04	(0.08)	–	–	2.26	1.52	0.74	–	1.4	(0.1)	–	–
	K4	9,300	143	2.30	(0.06)	3.64	(0.15)	3.44	2.19	1.25	–	1.8	(0.1)	2.9	(0.1)
	K6	9,555	152	4.66	(0.26)	–	–	3.59	2.28	1.31	–	3.5	(0.1)	–	–
Mariana	M1	6,032	50.4	1.79[a]	(0.09)	–	–	–	–	1.15[b]	(0.43)	1.6[b]	(0.6)	–	–
	M2	10,850	50.4	4.80	(0.09)	5.05[a]	(0.80)	–	–	2.64[b]	(0.80)	1.8	(0.7)	1.9[b]	(1.6)

Note. Suffix -E in A2, A4, A5, and A6 represents that these $^{210}Pb_{ex}$ concentrations were measured at Edith Cowan University. The other Atacama Trench samples were measured at Japan Agency for Marine-Earth Science and Technology.
[a]Depth integration to 25 cm (Glud et al., 2013; Turnewitsch et al., 2014), and. [b]Turnewitsch et al. (2014).

cent to the Atacama, Kermadec and Mariana trenches were similar ranging from 1.4 (K7) to 2.1 (A7) and with an average of 1.7 ± 0.3 (Table 3). The focusing factors along the four hadal trench axes were derived by applying the same pelagic data and generally expressed elevated values, ranging from 1.3 (A2) to 3.5 (K6) and with an average of 2.3 ± 1.1 (Table 3). We cannot exclude different deficient ^{210}Pb inventories in waters above the respective trench regions due to intensified ^{210}Pb scavenging along the trench boundaries (e.g., Nozaki et al., 1997), effects of seasonal and local variabilities of primary productivity (Cochran, 1992) (Table 3). However, these effects are expected to be minor and the *t*-test for the focusing factors between abyssal plain group (A7, K7, and M1) and hadal trench groups (A10, A2, A3, A4, A5, A6, KK1, KK4, KK9, KK11, K4, K6, and M2) resulted in p-value of 0.06, supporting the concept of intensified focusing along trench axes. Statistically, $^{210}Pb_{ex}$ inventory between the abyssal plain group and hadal trench group were different (0.002 in p-value), indicating that downslope transport of sediment parcels with high $^{210}Pb_{ex}$ concentration contribute to the observed elevated inventory of $^{210}Pb_{ex}$ in the hadal environments. The generally elevated focusing factors along the hadal trench axes suggest downslope material transport toward the trench interior even during periods without mass-wasting events (Figure 4a). A few hadal sites with relatively low focusing factors (i.e., 1.7–1.8 at A2; Table 3) could potentially imply limited focusing or winnowing driven by hydrography interacting with local bathymetric structures (Turnewitsch et al., 2014). Particle organic carbon flux and the removal fraction of ^{210}Pb in the water column have a generally strong relation (Moore & Dymondt, 1988). However, in our investigations there was no strong relationships between the derived annual
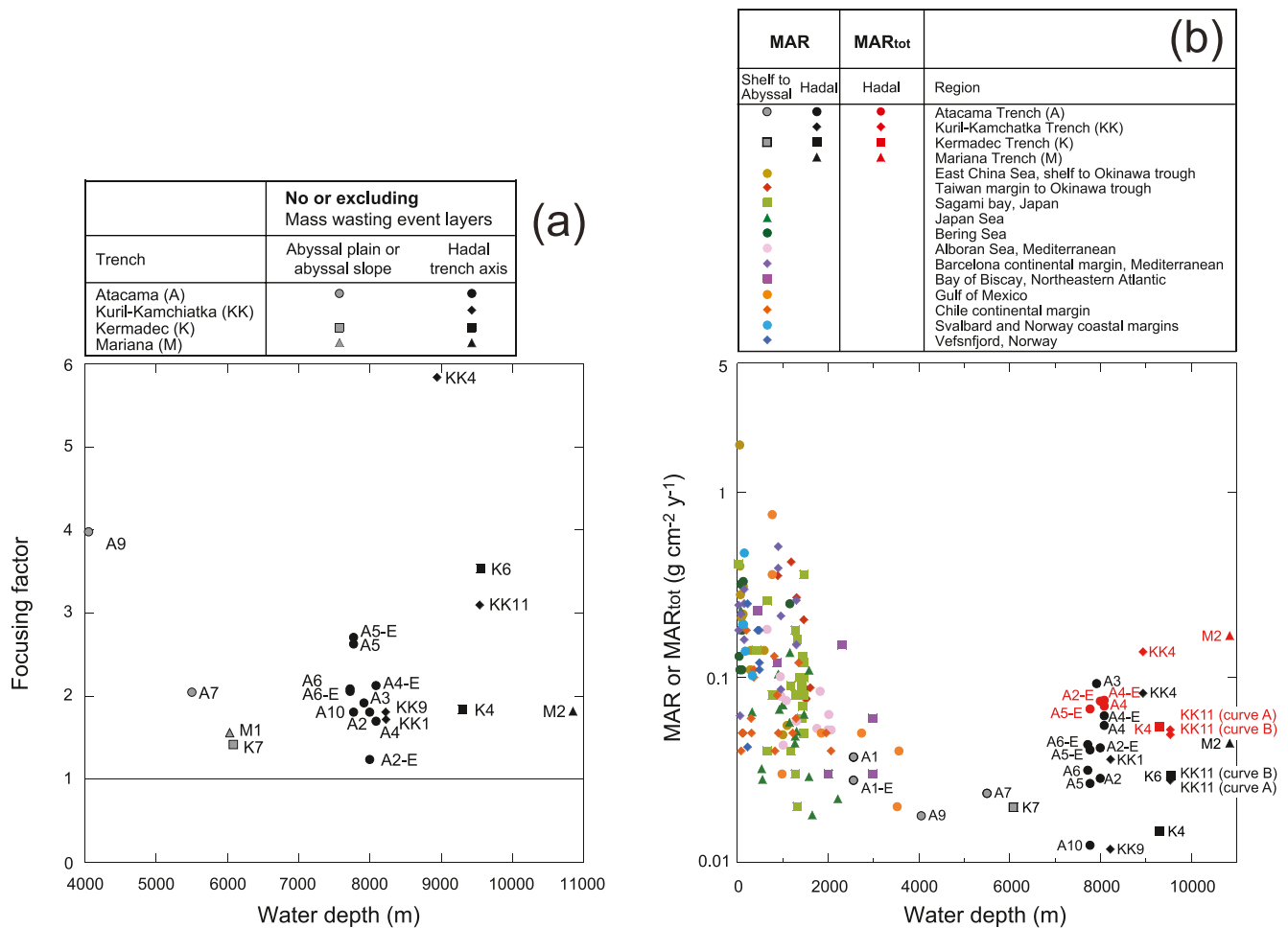
Figure 4. (a) The derived focusing factor for the targeted sites ignoring sedimentary depositions mediated by mass-wasting event layers as identified by profiles of $^{210}Pb_{ex}$ and total organic carbon distribution. (b) Mass Accumulation Rates (MARs) as a function of water depth for the compiled data include studies from: East China Sea shelf to Okinawa trough (Oguri et al., 2003), Taiwan margin to Okinawa trough (Chung & Chang, 1995), Sagami Bay (Kato et al., 2003), Japan Sea (Hong et al., 1997), Bering Sea (Oguri et al., 2012), Alboran Sea (Masqué et al., 2003), Barcelona continental margin (Sanchez-Cabeza et al., 1999), Bay of Biscay (Radakovitch & Heussner, 1999), Gulf of Mexico (Yeager et al., 2004), Chile continental margin (Muñoz et al., 2004), Svalbard and Norway coastal margins (Glud et al., 1998), Vefsnfjord (Heldal et al., 2021) and the current study. For hadal settings, the abbreviations indicate the respective trenches and sites as outlined in Table 1. Curve A and B represents shallower and deeper $^{210}Pb_{ex}$ decline curves, respectively (see Figure 3a). Suffix -E after A in the plots represents that the $^{210}Pb_{ex}$ concentrations was measured at Edith Cowan University. The others without suffix were measured at Japan Agency for Marine-Earth Science and Technology (A, K, and M) and the Scottish Universities Environmental Research Centre (KK), respectively. MARs of KK11 are calculated from the upper and the lower $^{210}Pb_{ex}$ decline curves.

net primary productivity and the focusing factor at the investigated hadal trench ($R^2 = 0.1$; Table 3). This result suggests that the $^{210}Pb_{ex}$ inventory in the hadal trench axis is not only linked to the net primary productivity but also to local deposition dynamics and secondary depositions. To compare MAR (and MAR_{tot}) in hadal settings to other marine settings, we compiled data from a wide range of environments. As expected, the data clearly demonstrate a gradual decline in MAR from the coastal regions across continental slopes and toward the abyssal plains (Figure 4b). However, the derived SR and MAR for hadal sites were elevated compared to the MAR for many continental slopes, even without including sediment layers deposited during mass-wasting events (Figure 4b), and generally exceed values from abyssal plains (Figure 4b, and Table 2). These findings suggest considerable material focusing along trench axes that is presumably mediated by gravity driven, near-bed, downslope material transport that is potentially modulated by tidal-driven internal waves or seiche (Taira et al., 2004; Turnewitsch et al., 2014; van Haren, 2020). Seven hadal sites had distinct records of mass wasting (A2, A4, A5, KK4, KK11, K4, and M2), and inclusion of $^{210}Pb_{ex}$ inventories from these deposits increased the MAR by factors of 1.2–3.8 (Figure 4b). The importance of mass wasting for the re-deposition of material in hadal trenches has been demonstrated previously (Bao et al., 2018; Itou et al., 2000; Nozaki & Ohta, 1993), and we identified 7 mass-wasting

event layers during the past ~150 years in 18 cores collected from the four trenches. So, on average mass-wasting events in these trenches occurred 0.045 times per year. Although mass-wasting events appear to be infrequent, they can apparently be responsible for marked local enhancement of the deposition along trench axes (Figure 4b). Additionally, our assessments also suggest that trenches are characterized by continuous accumulation of material focusing, even during periods without mass wasting (Figure 4b). Both the continuous and the erratic enhancement of material deposition might have important implications for the balance between microbial mineralization and burial of organic material and thereby long-term carbon sequestration in trench regions and the deep sea in general (Zabel et al., 2022).

### 4.3. Deposition of Organic Carbon in Hadal Trenches

Hadal trench sediments exhibit 2–5 times higher microbial mineralization rates compared to adjacent abyssal plain sediments (Glud et al., 2013; Luo et al., 2019; Wenzhöfer et al., 2016) and benthic hadal mineralization rates generally correlate well to net primary productivity in the surface ocean (Glud et al., 2021). The four targeted trench regions underly surface waters of very different net primary productivity (Table 1; from 50.4 to 449 gC m^{-2} y^{-1}), but there was no apparent relationship between the net primary productivity at the surface ocean and MAR ($R^2 = 0.08$) or OCDR ($R^2 = 0.2$) in the hadal environments (Tables 1 and 2). The deposition rates of organic carbon exhibited extensive site-specific variations (Figure S6 in Supporting Information S1). These observations suggest that deposition dynamics are strongly modulated by local bathymetry and are enhanced during mass-wasting events. Generally, the variability in OCDR is mainly caused by differences in SR and MAR rather than the TOC content (Table 2). For instance, variation in SR and MAR along the hadal Atacama Trench ranges by more than 7 fold (0.012–0.093 g cm^{-2} y^{-1}), while the variation in TOC content is less than 3 fold (0.39%–0.94%) (Table 2). The variability imposed by the highly complex bathymetry and corresponding geomorphology of subducting trenches (Kioka et al., 2019a; Stewart & Jamieson, 2018) underpin the challenge of extrapolating single point measurements to an entire trench system, let alone to hadal trenches in general. Inclusion of contributions from local, unpredictable mass-wasting events clearly further enhance the encountered variations of MAR and OCDR along the trench axis (Table 2, Figure 4b; Figure S7 in Supporting Information S1).

Mass-wasting events have been documented to facilitate high input of terrestrial organic carbon to hadal trenches in proximity of larger land masses (Luo et al., 2019). But for the Atacama and Kermadec trench axes, the main origin of organic carbon is estimated to be marine phytoplankton as inferred from stable carbon isotope ratio (δ^{13}C) (Xu et al., 2021). But the δ^{13}C values of organic carbon in the two trenches exhibit extensive variations and also layers with distinctly lower δ^{13}C values suggesting occasional deposition of mainly terrigenous organic carbon that might be related to mass-wasting events (Xu et al., 2021). The spatiotemporal variations in deposition rates and in sources of deposited organic carbon presumably induce highly variable mineralization and burial rates within and between different trench systems.

4.4. Accumulation of Organic Carbon in Hadal Trenches

Burial or retention of organic carbon in marine sediments are generally correlated with MAR (Canfield, 1994). In regions with low MAR, most of the deposited organic material is efficiently mineralized by aerobic microbial respiration. However, increasing deposition of organic carbon intensifies microbial mineralization and reduces the benthic O$_2$ availability whereby carbon mineralization to a larger extent is mediated by less efficient anaerobic mineralization. This process generally leads to relatively higher organic carbon accumulation at such settings (Burdige, 2007). To estimate the relative accumulation of deposited organic material, we combined the derived deposition rate of organic carbon (D$_R$) with previously published measurements of benthic mineralization rate (M$_R$) as derived from benthic O$_2$ consumption rates for the three trench systems where such measurements are available (Glud et al., 2013, 2021). To covert the benthic O$_2$ consumption rates to organic carbon mineralization rates we assumed a Respiratory Quotient (RQ) for the benthic mineralization of 0.85 (Jørgensen et al., 2022) and assume that reduced equivalents from anaerobic mineralization is reoxidized by oxygen (Glud, 2008). The burial efficiency of organic carbon (R$_{OM}$) in the sediment record should then equal:

$$R_{\text{OM}} = \frac{D_R}{D_R + M_R} \cdot 100\,(\%) \tag{2}$$
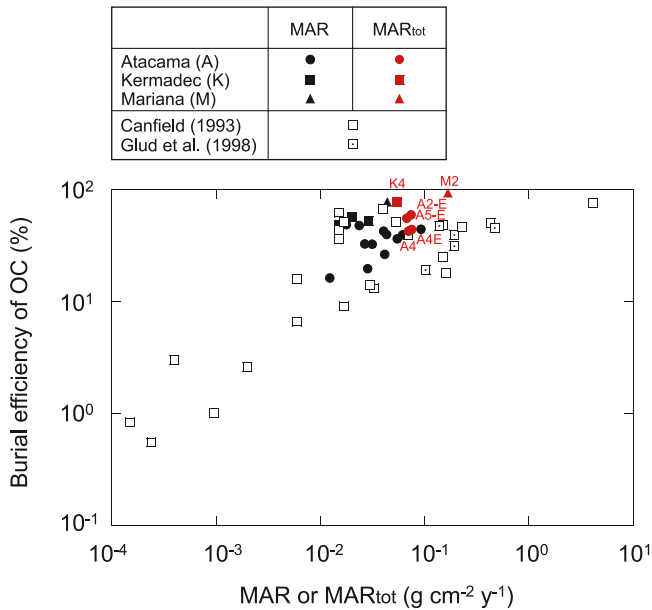
Figure 5. The burial efficiency of organic carbon as derived from deposition and mineralization rates versus the Mass Accumulation Rate (MAR) or total MAR (MAR$_{tot}$) quantified for a range of marine settings. The hadal data of the current study are plotted along with previous values collected at a depth range from 10 to 5,330 m compiled in Canfield (1993) and Glud et al. (1998).

The hadal values ranged from 12% (A10) to 77% (M2) with an overall average of 38 ± 16%, which compare to values from many coastal margins and shelf systems (Figure 5). This finding implies that even without mass wasting, hadal sediments could be important sites for carbon sequestration in the deep sea. The inclusion of deposits from mass wasting, makes this proposition even more explicit. The ~150 years averaged organic carbon accumulation rates including layers deposited during mass wasting as encountered at six sites enhanced the deposition of organic carbon by 1.1 (A4) to 3.3 (M2) times and accumulation of the organic carbon reached values between 40% (A4) and 92% (M2) (Table 4 and Figure 5). These assessments demonstrate that despite highly elevated microbial mineralization, hadal regions accumulate relatively large amounts of organic material. The current findings align with other recent investigations that demonstrating the importance of tectonic induced mass wasting for translocating organic carbon to the hadal environment (Bao et al., 2018; Kioka et al., 2019b; Zabel et al., 2022) and previous indirect evidence arguing for high carbon accumulation in hadal sediments (Luo et al., 2017; Xu et al., 2021), as well as recent findings of highly elevated sequestration of black carbon in some hadal settings (Zhang et al., 2022).

However, our study also documents large variation in the deposition rates and the burial efficiencies of organic carbon, both within and between different trench systems. This variability challenges quantitative extrapolation of our local studies to hadal trenches in general. Furthermore, the investigated sites only reflect conditions along or near the trench axis, that receive material from the trench slopes, and they are therefore not representative for the global hadal trench area that is estimated to cover 2.0×10^6 km^2 (Harris et al., 2014). Neither does our investigation include sites affected by large deposition events following mega quakes such as the Tohoku-Oki earthquake in 2011, where >1 Tg of organic carbon is estimated to have been translocated to the interior of the Japan Trench (Kioka et al., 2019a). Anyway, the organic carbon burial rates as derived from the difference between OCDR and M$_R$ at the 8 sites where both parameters were available, ranged between 0.8 and 6.7 ygC ym^{-2} y^{-1} with an average of 2.6 ± 1.9 ygC ym^{-2} y^{-1}. The global burial rate of organic carbon at water depths below 2,000 m covering an area of 311×10^6 km^2 has been assessed to 12 Tg yy^{-1} (Dunne et al., 2007) corresponding to 0.04 ygC ym^{-2} y^{-1}. Both estimates are admittingly associated with large error margins, but the carbon burial rates at the trench axis is ~70 times higher than the deep sea average. This strongly suggests that hadal trenches are quantitatively important sites for carbon sequestration and certainly accumulate proportionately more organic material than would be anticipated from their relatively small areal extent.

Table 4

Depth of Mass-Wasting Event, Total Organic Carbon Deposition Rate (OCDR) and Total OCDR (OCDR$_{tot}$) Derived From Total Mass Accumulation Rate (MAR$_{tot}$) and the Surface Total Organic Carbon (TOC) Content, and the Ratio of OCDR$_{tot}$/OCDR for the Respective Trench Sediments

Trench	Site	Depth at mass-wasting event layer (cm)	OCDR (gC m^{-2} y^{-1})	OCDR$_{tot}$ (gC m^{-2} y^{-1})	Ratio of OCDR$_{tot}$/ OCDR
Atacama	A2	5–12	1.12–1.64	6.64	3.6–5.9
	A4	7–10	3.15–3.56	4.05–4.36	1.1–1.4
	A5	10–15	1.78–2.71	4.52	1.7–2.5
Kermadec	K4	4–15	0.66	2.43	3.7
Mariana	M2	7–25	1.91	7.27	3.8

5. Conclusions and Perspectives

The current investigation demonstrates that for the past ~150 years SR and MAR and OCDR in four hadal trenches systems exceed values from the adjacent abyssal plain settings. The enhanced material transport is mediated by downslope focusing and mass-wasting events. The variations both within and between individual trenches are considerable, presumably due to local bathymetry, and spatiotemporal dynamics as induced by mass-wasting events. However, the sources and characteristics of the material reaching the trench axes are still poorly resolved (Lin et al., 2021; Luo et al., 2019; Xu et al., 2021). While the deposited organic material sustains high biological activity (Glud et al., 2021), it apparently also leads to considerable sequestration of organic material along the trench axes. The burial efficiency along the trench axes ranged from 16% to 77% without accounting for mass wasting, and 42%–93% when including contributions from mass-wasting events. These assessments scale with values encountered at oceanic margins or along continental slopes. The efficiency of anaerobic microbial degradation

in subsurface sediments enriched in organic material remain unknown and thus the timescale of hadal carbon retention require further insights on anaerobic mineralization at hadal depth. The study adds to the growing evidence that hadal trenches are complex (Stewart & Jamieson, 2018) and dynamic habitats, but quantitatively important sites for deposition and sequestration of organic carbon in the deep.

Data Availability Statement

The data set for this study is available from PANGAEA https://doi.pangaea.de/10.1594/PANGAEA.947927.

References

Aoyama, M., Hirose, K., & Igarashi, Y. (2006). Re-construction and updating our understanding on the global weapons tests ^{137}Cs fallout. *Journal of Environmental Monitoring*, *8*(4), 431–438. https://doi.org/10.1039/B512601K

Arai, K., Naruse, H., Miura, R., Kawamura, K., Hino, R., Ito, Y., et al. (2013). Tsunami-generated turbidity current of the 2011 Tohoku-Oki earthquake. *Geology*, *41*(11), 1195–1198. https://doi.org/10.1130/G34777.1

Athens, S. J. (1986). *Archaeological investigations at tarague beach, Guam. Report prepared for base civil engineering, Andersen air force base* (p. 113). International Archaeological Research Institute Inc.

Ausín, B., Bruni, E., Haghipour, N., Welte, C., Bernasconi, S. N., Eglinton, T. I., et al. (2021). Controls on the abundance, provenance and age of organic carbon buried in continental margin sediments. *Earth and Planetary Science Letters*, *558*(15), 116759. https://doi.org/10.1016/j.epsl.2021.116759

Bacon, M. P. (2005). Chapter 5 Reactive radionuclides as tracers of oceanic particle flux. In H. D. Livingston (Ed.), *Radioactivity in the environment book series volume 6, Marine Radioactivity* (pp. 139–165). Elsevier. https://doi.org/10.1016/S1569-4860(05)80006-3

Ballance, P. F., Follas, H. A., Forggatt, P. C., & Mikhailic, E. V. (2000). Continent-derived vitric mud and mafic-arc rocks in deep Kermadec Trench diamictons. *Journal of Sedimentary Research*, *70*(1), 140–150. https://doi.org/10.1306/2DC40905-0E47-11D7-8643000102C1865D

Bao, R., Strasser, M., McNichol, A. P., Haghipour, N., McIntyre, C., Wefer, G., & Eglinton, T. I. (2018). Tectonically-triggered sediment and carbon export to the hadal zone. *Nature Communications*, *9*(1), 121. https://doi.org/10.1038/s41467-017-02504-1

Barnett, P. R. O., Watson, J., & Connelly, D. (1984). A multiple corer for taking virtually undisturbed samples from shelf, bathyal and abyssal sediments. *Oceanologica Acta*, *7*(4), 399–408. https://doi.org/10.1017/S0269727000014846

Behrenfeld, M. J., & Falkowski, P. G. (1997). Photosynthetic rates derived from satellite-based chlorophyll concentration. *Limnology & Oceanography*, *42*, 1–20. https://doi.org/10.4319/lo.1997.42.1.0001

Benninger, L. K., Aller, R. C., Cochran, J. K., & Turekian, K. K. (1979). Effects of biological sediment mixing on the ^{210}Pb chronology and trace metal distribution in a Long Island Sound sediment core. *Earth and Planetary Science Letters*, *43*(2), 241–259. https://doi.org/10.1016/0012-821X(79)90208-5

Berg, P., Swaney, D., Rysgaard, S., Thamdrup, B., & Fossing, H. (2007). A fast numerical solution to the general mass-conservation equation for solutes and solids in aquatic sediments. *Journal of Marine Research*, *65*(3), 317–343. https://doi.org/10.1357/002224007781567649

Berger, W. H., Fisher, K., Lai, G., & Wu, G. (1987). Ocean carbon flux: Global maps of primary production and export production. In C. R. Agegian (Ed.), *Biogeochemical cycling and fluxes between the deep euphotic zone and other oceanic realms, Research Report 88–1* (pp. 131–176). NOAA National Undersea Research Program.

Blair, N. E., & Aller, R. C. (2012). The fate of terrestrial organic carbon in the marine environment. *Annual Review of Marine Science*, *4*(1), 401–423. https://doi.org/10.1146/annurev-marine-120709-142717

Brandt, A., Brix, S., Riehl, T., & Malyutina, M. (2020). Biodiversity and biogeography of the abyssal and hadal Kuril-Kamchatka trench and adjacent NW Pacific deep-sea regions. *Progress in Oceanography*, *181*, 102232. https://doi.org/10.1016/j.pocean.2019.102232

Burdige, D. J. (2007). Preservation of organic matter in marine sediments: Controls, mechanisms, and an imbalance in sediment organic carbon budgets. *Chemical Reviews*, *107*(2), 467–485. https://doi.org/10.1021/cr050347q

Canfield, D. E. (1993). Organic matter oxidation in marine sediments. In R. Wollast, F. T. Mackenzie, & L. Chou (Eds.), *Interactions of C, N, P and S biogeochemical cycles and global change, 4. NATO ASI series I: Global environmental change* (pp. 332–363). NATO Scientific Affairs Division. https://doi.org/10.1007/978-3-642-76064-8

Canfield, D. E. (1994). Factors influencing organic carbon preservation in marine sediments. *Chemical Geology*, *114*(3), 315–329. https://doi.org/10.1016/0009-2541(94)90061-2

Carpenter, R., Peterson, M. L., & Bennett, J. T. (1982). ^{210}Pb-derived sediment accumulation and mixing rates for the Washington continental slope. *Marine Geology*, *48*(1–2), 135–164. https://doi.org/10.1016/0025-3227(82)90133-5

Chung, Y., & Chang, W. C. (1995). Pb-210 fluxes and sedimentation rates on the lower continental slope between Taiwan and the South Okinawa Trough. *Continental Shelf Research*, *15*(2), 149–164. https://doi.org/10.1016/0278-4343(94)E0023-F

Chung, Y., & Craig, H. (1973). Radium-226 in eastern equatorial Pacific. *Earth and Planetary Science Letters*, *17*(2), 306–318. https://doi.org/10.1016/0012-821X(73)90195-7

Chung, Y., & Craig, H. (1980). [226]Ra in the Pacific Ocean. *Earth and Planetary Science Letters*, *49*(2), 267–292. https://doi.org/10.1016/0012-821X(80)90072-2

Chung, Y., & Craig, H. (1983). [210]Pb in the Pacific: The GEOSECS measurements of particulate and dissolved concentrations. *Earth and Planetary Science Letters*, *65*(2), 406–432. https://doi.org/10.1016/0012-821X(83)90179-6

Clark, G., Anderson, A., & Wright, D. (2006). Human colonization of the Palau Islands, western Micronesia. *Journal of Island and Coastal Archaeology*, *1*(2), 215–232. https://doi.org/10.1080/15564890600831705

Cochran, J. K. (1992). The oceanic chemistry of the uranium- and thorium-series nuclides. In M. Ivanovich & R. S. Harmon (Eds.), *Uranium-series disequilibrium: Applications to earth, marine, and environmental sciences* (2nd ed., pp. 334–395). Clarendon Press.

Craig, H., Krishnaswami, S., & Somayajulu, B. L. K. (1972). [210]Pb-[226]Ra: Radioactive disequilibrium in the deep sea. *Earth and Planetary Science Letters*, *17*(2), 295–305. https://doi.org/10.1016/0012-821X(73)90194-5

Danovaro, R., Croce, N. D., Dell'Anno, A., & Pusceddu, A. (2003). A depocenter of organic matter at 7800 m depth in the SE Pacific Ocean. *Deep Sea Research Part I: Oceanographic Research Papers*, *50*(12), 1411–1420. https://doi.org/10.1016/j.dsr.2003.07.001

Danovaro, R., Gambi, C., & Croce, N. D. (2002). Meiofauna hotspot in the Atacama Trench, eastern south Pacific Ocean. *Deep Sea Research Part I: Oceanographic Research Papers*, *49*(5), 843–857. https://doi.org/10.1016/S0967-0637(01)00084-X

Davis, R. B., Hess, C. T., Norton, S. A., Hanson, D. W., Hoagland, L. D., & Anderson, D. S. (1984). ^{137}Cs and ^{210}Pb dating of sediment from saft-water lakes in new England (U.S.A.) and Scandinavia, a failure of ^{137}Cs dating. *Chemical Geology*, *44*(1–3), 151–185. https://doi.org/10.1016/0009-2541(84)90071-8

DeMaster, D. J., & Cochran, J. K. (1982). Particle mixing rates in deep-sea sediments determined from excess ^{210}Pb and ^{32}Si profiles. *Earth and Planetary Science Letters*, *61*(2), 257–271. https://doi.org/10.1016/0012-821X(82)90057-7

DeMaster, D. J., McKee, B. A., Nittrouer, C. A., Jiangchu, Q., & Guodong, C. (1985). Rates of sediment accumulation and particle reworking based on radiochemieal measurements from continental shelf deposits in the East China Sea. *Continental Shelf Research*, *4*(1–2), 143–158. https://doi.org/10.1016/0278-4343(85)90026-3

Dunne, J. P., Sarmiento, J. L., & Gnanadesikan, A. (2007). A synthesis of global particle export from the surface ocean and cycling through the ocean interior and on the seafloor. *Global Biogeochemical Cycles*, *21*(4), GB4006. https://doi.org/10.1029/2006GB002907

Francois, R., Frank, M., Rutgers van der Loeff, M. M., & Bacon, M. P. (2004). ^{230}Th normalization: An essential tool for interpreting sedimentary fluxes during the late Quaternary. *Paleoceanography*, *19*(1), PA1018. https://doi.org/10.1029/2003PA000939

Fuller, C. C., van Geen, A., Baskaran, M., & Anima, R. (1999). Sediment chronology in San Francisco Bay, California, defined by, ^{210}Pb, ^{234}Th, ^{137}Cs and $^{239, 240}$Pu. *Marine Chemistry*, *64*(1), 7–27. https://doi.org/10.1016/S0304-4203(98)00081-4

Gallo, N. D., Cameron, J., Hardy, K., Fryer, P., Bartlett, D. H., & Levin, L. A. (2015). Submersible- and lander-observed community patterns in the Mariana and New Britain trenches: Influence of productivity and depth on epibenthic and scavenging communities. *Deep Sea Research Part I: Oceanographic Research Papers*, *99*, 119–133. https://doi.org/10.1016/j.dsr.2014.12.012

GEBCO Bathymetric Compilation Group. (2021). The GEBCO_2021 Grid—A continuous terrain model of the global oceans and land [Dataset]. Global ocean & land terrain models. https://doi.org/10.5285/c6612cbe-50b3-0cff-e053-6c86abc09f8f

Gebruk, A. V., Kremenetskaia, A., & Rouse, G. W. (2020). A group of species "Psychropotes longicauda" (Psychropotidae, Elasipodida, Holothuroidea) from the Kuril-Kamchatka Trench area (North-West Pacific). *Progress in Oceanography*, *180*, 102222. https://doi.org/10.1016/j.pocean.2019.102222

Glud, R. N. (2008). Oxygen dynamics of marine sediments. *Marine Biology Research*, *4*(4), 243–289. https://doi.org/10.1080/17451000801888726

Glud, R. N., Berg, P., Thamdrup, B., Larsen, M., Stewart, H. A., Jamieson, A. J., et al. (2021). Hadal trenches are dynamic hotspots for early diagenesis in the deep sea. *Communications Earth & Environment*, *2*(1), 21. https://doi.org/10.1038/s43247-020-00087-2

Glud, R. N., Holby, O., Hoffmann, F., & Canfield, D. E. (1998). Benthic mineralization and exchange in Arctic sediments (Svalbard, Norway). *Marine Ecology Progress Series*, *173*, 237–251. https://doi.org/10.3354/meps173237

Glud, R. N., Wenzhöfer, F., Middelboe, M., Oguri, K., Turnewitsch, R., Canfield, D. E., & Kitazato, H. (2013). High rates of microbial carbon turnover in sediments in the deepest oceanic trench on Earth. *Nature Geoscience*, *6*(4), 284–288. https://doi.org/10.1038/ngeo1773

Harden, S. L., DeMaster, D. J., & Nittrouer, C. A. (1992). Developing sediment geochronologies for high-latitude continental shelf deposits: A radiochemical approach. *Marine Geology*, *103*(1), 69–97. https://doi.org/10.1016/0025-3227(92)90009-7

Harris, P. T., Macmillan-Lawler, M., Rupp, J., & Baker, E. K. (2014). Geomorphology of the oceans. *Marine Geology*, *352*, 4–24. https://doi.org/10.1016/j.margeo.2014.01.011

Heaton, T. J., Köhler, P., Butzin, M., bard, E., Reimer, R. W., Austin, W. E. N., et al. (2020). Marine20—The marine radiocarbon age calibration curve (0–55, 000 cal BP). *Radiocarbon*, *62*(4), 779–820. https://doi.org/10.1017/RDC.2020.68

Heldal, H. E., Helvik, L., Appleby, P., Haanes, H., Volynkin, A., Jensen, H., & Lepland, A. (2021). Geochronology of sediment cores from the Vefsnfjord, Norway. *Marine Pollution Bulletin*, *170*, 112683. https://doi.org/10.1016/j.marpolbul.2021.112683

Hirose, K., Igarashi, Y., & Aoyama, M. (2008). Analysis of the 50-year records of the atmospheric deposition of long-lived radionuclides in Japan. *Applied Radiation and Isotopes*, *66*(11), 1675–1678. https://doi.org/10.1016/j.apradiso.2007.09.019

Hong, G., Kim, S., Chung, C., Kang, D.-J., Shin, D.-H., Lee, H., & Han, S.-J. (1997). ^{210}Pb-derived sediment accumulation rates in the southwestern East Sea (Sea of Japan). *Geo-Marine Letters*, *17*(2), 126–132. https://doi.org/10.1007/s003670050017

Ichino, M. C., Clark, M. R., Drazen, J. C., Jamieson, A., Jones, D. O., Martin, A. P., et al. (2015). The distribution of benthic biomass in hadal trenches: A modelling approach to investigate the effect of vertical and lateral organic matter transport to the seafloor. *Deep Sea Research Part I: Oceanographic Research Papers*, *100*, 21–33. https://doi.org/10.1016/j.dsr.2015.01.010

Iijima, K., Yasukawa, K., Fujinaga, K., Nakamura, K., Machida, S., Takaya, Y., et al. (2016). Discovery of extremely REY-rich mud in the western North Pacific Ocean. *Geochemical Journal*, *50*(6), 557–573. https://doi.org/10.2343/geochemj.2.0431

Ikehara, K., Kanamatsu, T., Nagahashi, Y., Strasser, M., Fink, H., Usami, K., et al. (2016). Documenting large earthquakes similar to the 2011 Tohoku-oki earthquake from sediments deposited in the Japan Trench over the past 1500 years. *Earth and Planetary Science Letters*, *445*, 48–56. https://doi.org/10.1016/j.epsl.2016.04.009

Ikehara, K., Usami, K., Irino, T., Omura, A., Jenkins, R. G., & Ashi, J. (2021). Characteristics and distribution of the event deposits induced by the 2011 Tohoku-oki earthquake and tsunami offshore of Sanriku and Sendai, Japan. *Sedimentary Geology*, *411*, 105791. https://doi.org/10.1016/j.sedgeo.2020.105791

Ikehara, K., Usami, K., & Kanamatsu, T. (2020). Repeated occurrence of surface-sediment remobilization along the landward slope of the Japan Trench by great earthquakes. *Earth Planets and Space*, *72*(1), 114. https://doi.org/10.1186/s40623-020-01241-y

Itoh, M., Kawamura, K., Kitahashi, T., Kojima, S., Katagiri, H., & Shimanaga, M. (2011). Bathymetric patterns of meiofaunal abundance and biomass associated with the Kuril and Ryukyu trenches, western North Pacific Ocean. *Deep Sea Research Part I: Oceanographic Research Papers*, *58*(1), 86–97. https://doi.org/10.1016/j.dsr.2010.12.004

Itou, M., Matsumura, I., & Noriki, S. (2000). A large flux of particulate matter in the deep Japan Trench observed just after the 1994 Sanriku-Oki earthquake. *Deep Sea Research Part I: Oceanographic Research Papers*, *47*(10), 1987–1998. https://doi.org/10.1016/S0967-0637(00)00012-1

Jażdżewska, A. (2015). Kuril–Kamchatka deep sea revisited—Insights into the amphipod abyssal fauna. *Deep Sea Research Part II: Topical Studies in Oceanography*, *111*, 294–300. https://doi.org/10.1016/j.dsr2.2014.08.008

Jeong, K. S., Kang, J. K., Lee, K. Y., Jung, H. S., Chi, S. B., & Ahn, S. J. (1996). Formation and distribution of manganese nodule deposit in the northwestern margin of Clarion-Clipperton fracture zones, northeast equatorial Pacific. *Geo-Marine Letters*, *16*(2), 123–131. https://doi.org/10.1007/BF02202607

Jørgensen, B. B., Wenzhöfer, F., Egger, M., & Glud, R. N. (2022). Sediment oxygen consumption: Role in the global marine carbon cycle. *Earth-Science Reviews*, *228*, 103987. https://doi.org/10.1016/j.earscirev.2022.103987

Kamenev, G. M., Mordukhovich, V. V., Alalykina, I. L., Chernyshev, A. V., & Maiorova, A. S. (2022). Macrofauna and nematode abundance in the abyssal and hadal zones of interconnected deep-sea ecosystems in the Kuril Basin (Sea of Okhotsk) and the Kuril-Kamchatka Trench (Pacific Ocean). *Frontiers in Marine Science*, *9*, 812464. https://doi.org/10.3389/fmars.2022.812464

Kato, Y., Kitazato, H., Shimanaga, M., Nakatsuka, T., Shirayama, Y., & Masuzawa, T. (2003). ^{210}Pb and ^{137}Cs in sediments from Sagami Bay, Japan: Sedimentation rates and inventories. *Progress in Oceanography*, *57*(1), 77–95. https://doi.org/10.1016/S0079-6611(03)00052-1

Kawagucci, S., Yoshida, Y. T., Noguchi, T., Honda, M. C., Uchida, H., Ishibashi, H., et al. (2012). Disturbance of deep-sea environments induced by the M9.0 Tohoku Earthquake. *Scientific Reports*, *2*(1), 270. https://doi.org/10.1038/srep00270

Kawamura, K., Sasaki, T., Kanamatsu, T., Sakaguchi, A., & Ogawa, Y. (2012). Large submarine landslides in the Japan Trench: A new scenario for additional tsunami generation. *Geophysical Research Letters*, *39*(5), L05308. https://doi.org/10.1029/2011GL050661

Kioka, A., Schwestermann, T., Moernaut, J., Ikehara, K., Kanamatsu, T., Eglinton, T. I., & Strasser, M. (2019b). Event stratigraphy in a hadal oceanic trench: The Japan Trench as sedimentary archive recording recurrent giant subduction zone earthquakes and their role in organic carbon export to the deep sea. *Frontiers of Earth Science*, *7*, 319. https://doi.org/10.3389/feart.2019.00319

Kioka, A., Schwestermann, T., Moernaut, J., Ikehara, K., Kanamatsu, T., McHugh, C., et al. (2019a). Megathrust earthquake drives drastic organic carbon supply to the hadal trench. *Scientific Reports*, *9*(1), 1553. https://doi.org/10.1038/s41598-019-38834-x

Klaminder, J., Appleby, P., Crook, P., & Renberg, I. (2012). Post-deposition diffusion of ^{137}Cs in lake sediment: Implications for radiocaesium dating. *Sedimentology*, *59*(7), 2259–2267. https://doi.org/10.1111/j.1365-3091.2012.01343.x

Koide, M., Soutar, A., & Goldberg, E. D. (1972). Marine geochronology with ^{210}Pb. *Earth and Planetary Science Letters*, *14*(3), 442–446. https://doi.org/10.1016/0012-821X(72)90146-X

Koller, H., Dworschak, P. C., & Abed-Navandi, D. (2006). Burrows of *Pestarella tyrrhena* (Decapoda: Thallasinidea): Hot spots for Nematoda, Foraminifera and bacterial densities. *Journal of the Marine Biological Association of the United Kingdom*, *86*(5), 1113–1122. https://doi.org/10.1017/S0025315406014093

Krishnaswami, L. D., Martin, J. M., & Meybeck, M. (1971). Geochronology of lake sediments. *Earth and Planetary Science Letters*, *11*(1), 407–414. https://doi.org/10.1016/0012-821X(71)90202-0

Kusakabe, M., Inatomi, N., Takata, H., & Ikenoue, T. (2017). Decline in radiocesium in seafloor sediments off Fukushima and nearby prefectures. *Journal of Oceanography*, *73*(5), 529–545. https://doi.org/10.1007/s10872-017-0440-2

Leduc, D., & Rowden, A. A. (2018). Nematode communities in sediments of the Kermadec Trench, Southwest Pacific Ocean. *Deep Sea Research Part I: Oceanographic Research Papers*, *134*, 23–31. https://doi.org/10.1016/j.dsr.2018.03.003

Lin, G., Luo, M., Chen, L., Chen, Y., & Chen, D. (2021). Geochemistry and mineralogy of the sediments in the New Britain shelf-trench continuum, offshore Papua New Guinea: Insights into sediment provenance and burial in hadal trenches. *Deep Sea Research Part I: Oceanographic Research Papers*, *177*, 103621. https://doi.org/10.1016/j.dsr.2021.103621

Luo, M., Giskes, J., Chen, L., Scholten, J., Pan, B., Lin, G., & Chen, D. (2019). Sources, degradation, and transport of organic matter in the New Britain Shelf-Trench continuum, Papua New Guinea. *Journal of Geophysical Research: Biogeosciences*, *124*(6), 1680–1695. https://doi.org/10.1029/2018JG004691

Luo, M., Giskes, J., Chen, L., Shi, X., & Chen, D. (2017). Provenances, distribution, and accumulation of organic matter in the southern Mariana Trench rim and slope: Implication for carbon cycle and burial in hadal trenches. *Marine Geology*, *386*, 98–106. https://doi.org/10.1016/j.margeo.2017.02.012

Masqué, P., Fabres, J., Canals, M., Sanchez-Cabeza, J. A., Vidal-Sanchez, A., Cacho, I., et al. (2003). Accumulation rates of major constituents of hemipelagic sediments in the deep Alboran Sea: A centennial perspective of sedimentary dynamics. *Marine Geology*, *193*(3), 207–233. https://doi.org/10.1016/S0025-3227(02)00593-5

McHugh, C. M., Kanamatsu, T., Seeber, L., Bopp, R., Cormier, M.-H., & Usami, K. (2016). Remobilization of surficial slope sediment triggered by the A.D. 2011 M$_w$ 9 Tohoku-Oki earthquake and tsunami along the Japan Trench. *Geology*, *44*(5), 391–394. https://doi.org/10.1130/G37650.1

McHugh, C. M., Seebar, L., Rasbury, T., Strasser, M., Kioka, A., Kanamatsu, T., et al. (2020). Isotopic and sedimentary signature of megathrust ruptures along the Japan subduction margin. *Marine Geology*, *428*, 106283. https://doi.org/10.1016/j.margeo.2020.106283

McKee, B. A., Nittrouer, C. A., & DeMaster, D. J. (1983). Concepts of sediment deposition and accumulation applied to the continental shelf near the mouth of the Yangtze River. *Geology*, *11*(11), 631–633. https://doi.org/10.1130/0091-7613(1983)11<631:COSDAA>2.0.CO;2

Moore, W. S., & Dymondt, J. (1988). Correlation of ^{210}Pb removal with organic carbon fluxes in the Pacific Ocean. *Nature*, *331*(6154), 339–341. https://doi.org/10.1038/331339a0

Muñoz, P., Lange, C. B., Cutiérrez, D., Hebbeln, D., Salamanca, M. A., Dezileau, L., et al. (2004). Recent sedimentation and mass accumulation rates based on ^{210}Pb along the Peru-Chile continental margin. *Deep Sea Research Part II: Topical Studies in Oceanography*, *51*(20), 2523–2541. https://doi.org/10.1016/j.dsr2.2004.08.015

Nittrouer, C. A., DeMaster, D. J., McKee, B. A., Cutshall, H. H., & Larsen, L. (1984). The effect of sediment mixing on Pb-210 accumulation rates for the Washington continental shelf. *Marine Geology*, *54*(3), 201–221. https://doi.org/10.1016/0025-3227(84)90038-0

Noguchi, T., Tanikawa, W., Hirose, T., Lin, W., Kawagucci, S., Yoshida-Takashima, Y., et al. (2011). Dynamic process of turbidity generation triggered by the 2011 Tohoku-Oki earthquake. *Geochemistry, Geophysics, Geosystems*, *13*(11), Q11003. https://doi.org/10.1029/2012GC004360

Nozaki, Y., Cochran, K., Turekian, K. K., & Keller, G. (1977). Radiocarbon and ^{210}Pb distribution in submersible-taken deep-sea cores from Project FAMOUS. *Earth and Planetary Science Letters*, *34*(2), 167–173. https://doi.org/10.1016/0012-821X(77)90001-2

Nozaki, Y., & Ohta, Y. (1993). Rapid and frequent turbidite accumulation in the bottom of Izu-Ogasawara Trench: Chemical and radiochemical evidence. *Earth and Planetary Science Letters*, *120*(3), 345–360. https://doi.org/10.1016/0012-821X(93)90249-9

Nozaki, Y., Zhang, J., & Takeda, A. (1997). ^{210}Pb and ^{210}Po in the equatorial Pacific and the Bering Sea: The effects of biological productivity and boundary scavenging. *Deep Sea Research Part II: Topical Studies in Oceanography*, *44*(9), 2203–2220. https://doi.org/10.1016/S0967-0645(97)00024-6

Oguri, K., Furushima, Y., Toyofuku, T., Kasaya, T., Wakita, M., Watanabe, S., et al. (2016). Long-term monitoring of bottom environments of the continental slope off Otsuchi Bay, northeastern Japan. *Journal of Oceanography*, *72*(1), 151–166. https://doi.org/10.1007/s10872-015-0330-4

Oguri, K., Harada, N., & Tadai, O. (2012). Excess ^{210}Pb and ^{137}Cs concentrations, mass accumulation rates, and sedimentary processes on the Bering Sea continental shelf. *Deep Sea Research Part II: Topical Studies in Oceanography*, *61*, 193–204. https://doi.org/10.1016/j.dsr2.2011.03.007

Oguri, K., Kawamura, K., Sakaguchi, A., Toyofuku, T., Kasaya, T., Murayama, M., et al. (2013). Hadal disturbance in the Japan Trench induced by the 2011 Tohoku-Oki Earthquake. *Scientific Reports*, *3*(1), 1915. https://doi.org/10.1038/srep01915

Oguri, K., Matsumoto, E., Saito, Y., Yamada, M., & Iseki, K. (2003). Sediment accumulation rates and budgets of depositing particles of the East China Sea. *Deep Sea Research Part II: Topical Studies in Oceanography*, *50*(2), 513–528. https://doi.org/10.1016/S0967-0645(02)00465-4

Pattan, J. N., & Parthiban, G. (2007). Do manganese nodules grow or dissolve after burial? Results from the Central Indian Ocean Basin. *Journal of Asian Earth Sciences*, *30*(5–6), 696–705. https://doi.org/10.1016/j.jseaes.2007.03.003

Radakovitch, O., & Heussner, S. (1999). Fluxes and budget of ^{210}Pb on the continental margin of the Bay of Biscay (northeastern Atlantic). *Deep Sea Research Part II: Topical Studies in Oceanography*, *46*(10), 2175–2203. https://doi.org/10.1016/S0967-0645(99)00059-4

Reimer, P. J., Austin, W. E. N., Bard, E., Bayliss, A., Blackwell, P. G., Ramsey, C. B., et al. (2020). The IntCal20 northern hemisphere radiocarbon age calibration curve (0-55 cal kBP). *Radiocarbon*, *62*(4), 725–757. https://doi.org/10.1017/RDC.2020.41

Sanchez-Cabeza, J. A., Masqué, P., & Ani-Ragolta, I. (1998). ^{210}Pb and ^{210}Po analysis in sediments and soils by microwave acid digestion. *Journal of Radioanalytical and Nuclear Chemistry*, *227*(1–2), 19–22. https://doi.org/10.1007/bf02386425

Sanchez-Cabeza, J. A., Masqué, P., Ani-Ragolta, I., Merino, J., Frignani, M., Alvisi, F., et al. (1999). Sediment accumulation rates in the southern Barcelona continental margin (NW Mediterranean Sea) derived from ^{210}Pb and ^{137}Cs Chronology. *Progress in Oceanography*, *44*(1–3), 313–332. https://doi.org/10.1016/S0079-6611(99)00031-2

Schauberger, C., Middelboe, M., Larsen, M., Peoples, L. M., Bartlett, D. H., Kirpekar, F., et al. (2021). Spatial variability of prokaryotic and viral abundances in the Kermadec and Atacama Trench regions. *Limnology & Oceanography*, *66*(6), 2095–2109. https://doi.org/10.1002/lno.11711

Schwestermann, T., Eglinton, T. I., Haghipour, N., McNichol, A. P., Ikehara, K., & Strasser, M. (2021). Event-dominated transport, provenance, and burial of organic carbon in the Japan Trench. *Earth and Planetary Science Letters*, *563*, 116870. https://doi.org/10.1016/j.epsl.2021.116870

Schwestermann, T., Huang, J., Konzett, J., Kioka, A., Wefer, G., Ikehara, K., et al. (2020). Multivariate statistical and multiproxy constraints on earthquake-triggered sediment remobilization processes in the central Japan Trench. *Geochemistry, Geophysics, Geosystems*, *21*(6), e2019GC008861. https://doi.org/10.1029/2019GC008861

Shimabukuro, M., Zeppilli, D., Leduc, D., Wenzhöfer, F., Berg, P., Rowden, A. A., & Glud, R. N. (2022). Intra- and inter-spatial variability of meiofauna in hadal trenches is linked to microbial activity and food availability. *Scientific Reports*, *12*(1), 4338. https://doi.org/10.1038/s41598-022-08088-1

Southon, J., Kashgarian, M., Fontugne, M., Metivier, B., & Yim, W. W.-S. (2016). Marine reservoir corrections for the Indian Ocean and Southeast Asia. *Radiocarbon*, *44*(1), 167–180. https://doi.org/10.1017/S0033822200064778

Stewart, H. A., & Jamieson, A. J. (2018). Habitat heterogeneity of hadal trenches: Considerations and implications for future studies. *Progress in Oceanography*, *161*, 47–65. https://doi.org/10.1016/j.pocean.2018.01.007

Stuiver, M., & Polach, H. A. (1977). Discussion reporting of ^{14}C data. *Radiocarbon*, *19*(3), 355–363. https://doi.org/10.1017/S0033822200003672

Taira, K., Kitagawa, S., Yamashiro, T., & Yanagimoto, D. (2004). Deep and bottom currents in the Challenger Deep, Mariana Trench, measured with super-deep current meters. *Journal of Oceanography*, *60*(6), 919–926. https://doi.org/10.1007/s10872-005-0001-y

Thamdrup, B., Schauberger, C., Larsen, M., Trouche, B., Maignien, L., Arnaud-Haond, S., et al. (2021). Anammox bacteria drive fixed nitrogen loss in hadal trench sediments. *Proceedings of the National Academy of Sciences of the United States of America*, *118*(46), e2104529118. https://doi.org/10.1073/pnas.2104529118

Thomson, J., & Turekian, K. K. (1976). ^{210}Po and ^{210}Pb distributions in ocean water profiles from the eastern south Pacific. *Earth and Planetary Science Letters*, *32*(2), 297–303. https://doi.org/10.1016/0012-821X(76)90069-8

Todo, Y., Kitazato, H., Hashimoto, J., & Gooday, A. J. (2005). Simple Foraminifera Flourish at the Ocean's Deepest Point. *Science*, *307*(5710), 689. https://doi.org/10.1126/science.1105407

Tsumune, D., Aoyama, M., Hirose, K., Bryan, F. O., Lindsay, K., & Danabasoglu, G. (2011). Transport of ^{137}Cs to the Southern Hemisphere in an ocean general circulation model. *Progress in Oceanography*, *89*(1), 38–48. https://doi.org/10.1016/j.pocean.2010.12.006

Turnewitsch, R., Falahat, S., Stehjjlikova, J., Oguri, K., Glud, R. N., Middelboe, M., et al. (2014). Recent sediment dynamics in hadal trenches: Evidence for the influence of higher-frequency (tidal, near-intertidal) fluid dynamics. *Deep Sea Research Part I: Oceanographic Research Papers*, *90*, 125–138. https://doi.org/10.1016/j.dsr.2014.05.005

Turnewitsch, R., Reyss, J.-L., Chapman, D. C., Thomson, J., & Lampitt, R. S. (2004). Evidence for a sedimentary fingerprint of an asymmetric flow surrounding a short seamount. *Earth and Planetary Science Letters*, *222*(3), 1023–1036. https://doi.org/10.1016/j.epsl.2004.03.042

Usami, K., Ikehara, K., Kanamatsu, T., Kioka, A., Schwestermann, T., & Strasser, M. (2021). The link between upper-slope submarine landslides and mass transport deposits in the hadal trenches. Understanding and reducing landslide disaster risk. In *Understanding and reducing landslide disaster risk. Volume 1 Sendai landslide partnerships and Kyoto landslide commitment* (pp. 361–367). Springer Nature Switzerland AG. https://doi.org/10.1007/978-3-030-60196-6_26

Usami, K., Ikehara, K., Kanamatsu, T., & McHugh, C. M. (2018). Supercycle in great earthquake recurrence along the Japan Trench over the last 4000 years. *Geoscience Letters*, *5*(1), 11. https://doi.org/10.1186/s40562-018-0110-2

van Haren, H. (2020). Challenger deep internal wave turbulence events. *Deep Sea Research Part I: Oceanographic Research Papers*, *165*, 103400. https://doi.org/10.1016/j.dsr.2020.103400

Wang, X.-C., Druffel, E. R. M., & Lee, C. (1996). Radiocarbon in organic compound classes in particulate organic matter and sediment in the deep northeast Pacific Ocean. *Geophysical Research Letters*, *23*(24), 3583–3586. https://doi.org/10.1029/96GL03423

Wenzhöfer, F., Oguri, K., Middelboe, M., Turnewitsch, R., Toyofuku, T., Kitazato, H., & Glud, R. N. (2016). Benthic carbon mineralization in hadal trenches: Assessment by in situ O_2 microprofile measurements. *Deep Sea Research Part I: Oceanographic Research Papers*, *116*, 276–286. https://doi.org/10.1016/j.dsr.2016.08.013

Weston, J. N., & Jamieson, A. J. (2022). The multi-ocean distribution of the hadal amphipod, *Hirondellea dubia* Dahl, 1959 (crustacea, amphipoda). *Frontiers in Marine Science*, *9*, 824640. https://doi.org/10.3389/fmars.2022.824640

Wolff, T. (1970). The concept of the hadal or ultra-abyssal fauna. *Deep-Sea Research and Oceanographic Abstracts*, *17*(6), 983–1003. https://doi.org/10.1016/0011-7471(70)90049-5

Xu, Y., Li, X., Luo, M., Xiao, W., Fang, J., Rashid, H., et al. (2021). Distribution, source and burial of sedimentary organic carbon in Kermadec and Atacama trenches. *Journal of Geophysical Research: Biogeosciences*, *126*(5), e2020JG006189. https://doi.org/10.1029/2020JG006189

Yeager, K. M., Santschi, P. H., & Rowe, G. T. (2004). Sediment accumulation and radionuclide inventories ($^{239, 240}$Pu, ^{210}Pb and ^{234}Th) in the northern Gulf of Mexico, as influenced by organic matter and macrofaunal density. *Marine Chemistry*, *91*(1–4), 1–14. https://doi.org/10.1016/j.marchem.2004.03.016

Yokoyama, Y., Tims, S., Froehlich, M., Hirabayashi, S., Aze, T., Fifield, L. K., et al. (2022). Plutonium isotopes in the North Western Pacific sediments coupled with radiocarbon in corals recording precise timing of the Anthropocene. *Scientific Reports*, *12*(1), 10068. https://doi.org/10.1038/s41598-022-14179-w

Zabel, M., Glud, R. N., Sanei, H., Elvert, M., Page, T., Chuang, P.-C., et al. (2022). High carbon mineralization rates in subseafloor hadal sediments—Result of frequent mass wasting. *Geochemistry, Geophysics, Geosystems*, *23*(9), e2022GC10502. https://doi.org/10.1029/2022GC010502

Zhang, X., Xu, Y., Xiao, W., Zhao, M., Wang, Z., Wang, X., et al. (2022). The hadal zone is an important and heterogeneous sink of black carbon in the oceans. *Communications Earth & Environment*, *3*(1), 25. https://doi.org/10.1038/s43247-022-00351-7

References From the Supporting Information

Buruaem, L. M., de Castro, Í. B., Hortellani, M. A., Taniguchi, S., Fillmann, G., Sasaki, S. T., et al. (2013). Integrated quality assessment of sediments from harbour areas in Santos-São Vicente Estuarine System, Southern Brazil. *Estuarine, Coastal and Shelf Science*, *130*, 179–189. https://doi.org/10.1016/j.ecss.2013.06.006

Coimbra, J. C., Carreño, A. L., Geraque, E. A., & Eichler, B. B. (2007). Ostracode (Crustacea) from Cananéia-Iguape estuarine/lagoon system and geographical distribution of the mixohaline assemblages in southern and southeastern Brazil. *Iheringia Serie Zoologia*, *97*(3), 273–279. https://doi.org/10.1590/S0073-47212007000300010

Corzo, A., van Bergeijk, S. A., & García-Robledo, E. (2009). Effects of green macroalgal blooms on intertidal sediments: Net metabolism and carbon and nitrogen contents. *Marine Ecology Progress Series*, *380*, 81–93. https://doi.org/10.3354/meps07923

de Lima Ferreira, P. A., Siegle, E., Schettini, C. A. F., de Mahiques, M. M., & Figueira, R. C. L. (2015). Statistical validation of the model of diffusion-convection (MDC) of ^{137}Cs for the assessment of recent sedimentation rates in coastal systems. *Journal of Radioanalytical and Nuclear Chemistry*, *303*, 2059–2071. https://doi.org/10.1007/s10967-014-3622-z

Díaz, T. L., Rodrigues, A. R., & Eichler, B. B. (2014). Distribution of foraminifera in a subtropical Brazilian estuarine system. *Journal of Foraminiferal Research*, *44*(2), 90–108. https://doi.org/10.2113/gsjfr.44.2.90

Eichler, P. P. B., Eichler, B. B., Miranda, L. B., & Rodrigues, A. R. (2007). Modern foraminiferal facies in a subtropical estuarine channel Bertioga, São Paulo, Brazil. *Journal of Foraminiferal Research*, *37*(3), 234–247. https://doi.org/10.2113/gsjfr.37.3.234

Heidelberg, K. B., Nelson, W. C., Holm, J. B., Eisenkolb, N., Andrade, K., & Emerson, J. B. (2013). Characterization of eukaryotic microbial diversity in hypersaline Lake Tyrrell, Australia. *Frontiers in Microbiology*, *4*, 115. https://doi.org/10.3389/fmicb.2013.00115

Ligero, R. A., Barrera, M., & Casas-Ruiz, M. (2005). Levels of ^{137}Cs in muddy sediments on the seabed in the Bay of Cádiz (Spain). Part II. Model of vertical migration of ^{137}Cs. *Journal of Environmental Radioactivity*, *80*(1), 87–103. https://doi.org/10.1016/j.jenvrad.2004.06.006

Longmore, M. E., Torgersen, T., O'leary, B. M., & Luly, J. (1986). Cesium-137 redistribution in the sediments of the Playa, Lake Tyrrell, Northwestern Victoria. I. Stratigraphy and Cesium-137 mobility in the upper sediments. *Palaeogeography, Palaeoclimatology, Palaeoecology*, *54*(1–4), 181–195. https://doi.org/10.1016/0031-0182(86)90124-0

Nagaya, Y., & Nakamura, K. (1987). Artificial radionuclides in the Western Northwest Pacific (II): ^{137}Cs and $^{239, 240}$Pu inventories in water and sediment columns observed from 1980 to 1986. *Journal of the Oceanographical Society of Japan*, *43*(6), 345–355. https://doi.org/10.1007/BF02109287

Nozaki, Y., Yamada, M., Nakanishi, T., Nagaya, Y., Nakamura, K., Shitashima, K., & Tsubota, H. (1998). The distribution of radionuclides and some trace metals in the water columns of the Japan and Bonin trenches. *Oceanologica Acta*, *21*(3), 469–484. https://doi.org/10.1016/S0399-1784(98)80031-5

Papaspyrou, S., Diz, P., García-Robledo, E., Corzo, A., & Jimenez-Arias, J.-L. (2013). Benthic foraminiferal community changes and their relationship to environmental dynamics in inter tidal muddy sediments (Bay of Cádiz, SW Spain). *Marine Ecology Progress Series*, *490*, 121–135. https://doi.org/10.3354/meps10447

Robbins, J. A., McCall, P. L., Fisher, J. B., & Krezoski, J. R. (1979). Effects of deposit feeders on migration of ^{137}Cs in lake sediments. *Earth and Planetary Science Letters*, *42*(2), 277–287. https://doi.org/10.1016/0012-821X(79)90035-9

Saia, F. T., Damianovic, M. H. R. Z., Cattony, E. B. M., Brucha, B., Forsti, E., & Vazoller, R. F. (2007). Anaerobic biodegradation of pentachlorophenol in a fixed-film reactor inoculated with polluted sediment from Santos–São Vicente Estuary, Brazil. *Applied Microbiology and Biotechnology*, *75*(3), 665–672. https://doi.org/10.1007/s00253-007-0841-z